

Article

Adaptive Fuzzy-Based Fault-Tolerant Control of a Continuum Robotic System for Maxillary Sinus Surgery

Farzin Piltan ¹, Cheol-Hong Kim ² and Jong-Myon Kim ^{3,*}

¹ Department of Electrical, Electronics and Computer Engineering, University of Ulsan, Ulsan 44610, Korea; piltanfarzin@gmail.com

² School of Electronics and Computer Engineering, Chonnam National University, Gwangju 61186, Korea; chkim22@chonnam.ac.kr

³ School of IT Convergence, University of Ulsan, Ulsan 44610, Korea

* Correspondence: jmkim07@ulsan.ac.kr; Tel.: +82-52-259-2217

Received: 7 May 2019; Accepted: 14 June 2019; Published: 19 June 2019



Abstract: Continuum robots represent a class of highly sensitive, multiple-degrees-of-freedom robots that are biologically inspired. Because of their flexibility and accuracy, these robots can be used in maxillary sinus surgery. The design of an effective procedure with high accuracy, reliability, robust fault diagnosis, and fault-tolerant control for a surgical robot for the sinus is necessary to maintain the high performance and safety necessary for surgery on the maxillary sinus. Thus, a robust adaptive hybrid observation method using an adaptive, fuzzy auto regressive with exogenous input (ARX) Laguerre Takagi–Sugeno (T–S) fuzzy robust feedback linearization observer for a surgical robot is presented. To address the issues of system modeling, the fuzzy ARX–Laguerre technique is represented. In addition, a T–S fuzzy robust feedback linearization observer is applied to a fuzzy ARX–Laguerre to improve the accuracy of fault estimation, reliability, and robustness for the surgical robot in the presence of uncertainties. For fault-tolerant control in the presence of uncertainties and unknown conditions, an adaptive fuzzy observation-based feedback linearization technique is presented. The effectiveness of the proposed algorithm is tested with simulations. Experimental results show that the proposed method reduces the average position error from 35 mm to 2.45 mm in the presence of faults.

Keywords: continuum robot manipulator; maxillary sinus surgery; T–S fuzzy algorithm; variable structure algorithm; observation technique; fuzzy ARX–Laguerre system modeling; feedback linearization observer; adaptive technique; fault diagnosis; fault-tolerant control

1. Introduction

The maxillary sinus is a conic, hollow space in the bones of the face that connects to the nose. It is the largest cavity of air in the body, and its main function is mucus production. The maxillary sinus can experience many health issues, such as nasal polyps, maxillary sinusitis, and nasal sinus cysts, which can cause infections [1,2]. Task complexities, narrow geometry, and limited accessibility to the sinus creates several challenges for maxillary sinus surgery. Infection of a maxillary sinus causes pain and pressure (e.g., headache and toothache). Therefore, finding a good method for maxillary sinus surgery is important [3]. These techniques are divided into two main groups: (a) minimally invasive surgery, and (b) a non-invasive surgery technique. The creating an incision in the face, pain, and long recovery time are main challenges of the open sinus surgery. In most of cases, sinus surgery is performed as minimally invasive surgery [4]. The natural orifice transluminal endoscopic surgery (NOTES) is one of the important techniques for minimally invasive surgery. Despite the several

advantages of NOTES, surgeons still have challenges due to the narrow operating space. To improve the performance of endoscopic surgery, a number of continuum robots (e.g., concentric tube robots, tendon-driven robots, and soft robots) have been represented [3,4]. While concentric tube robots have several advantages, limited bending angle and small stiffness are two drawbacks of the technique [5]. Various tendon-driven robots have been developed by various researchers for surgery [3,6]. A soft robot is a promising technique for surgical techniques. This technique has been used in various surgery but it is not useful for maxillary sinus surgery [3,7]. Figure 1 illustrates the position of the maxillary sinus. Robot-assisted surgery is used to reduce surgeon's hand tremors, postoperative complications, and pain and to increase the precision of the actions performed during surgery. Robots have been widely used in many medical fields such as orthopedics, neurology, urology, and cardiology. Robot-assisted surgery is expanding its effects in the general medical field but has various challenges, such as non-linear behavior, the need for high-accuracy control, insertion depth perception, contact force feedback, and fault diagnosis. Various defects in robotic assistants can be categorized as actuator faults, sensor faults, and system faults. The actuator fault is affecting the continuum robot inputs. The actuator fault can be caused by abnormal operation or material aging and can drastically change the system behavior and operation. Therefore, a fault in a continuum robot motor's joint or operator can cause the actuator fault. Continuum robots are usually equipped with sensors to recognize the surrounding environment. Unfortunately, sensors are susceptible to faults and they might lead to task failure. In this paper, actuator and sensor fault detection, diagnosis, and tolerant control are analyzed. To analyze the condition of actuator and sensor faults in robot-assisted surgery, various monitoring techniques for robot conditions such as torque, voltage, current, and vibration have been reported [8–10]. This research exploits torque measurements because these signals are suitable for system and fault modeling, identification, estimation, and fault-tolerant control.

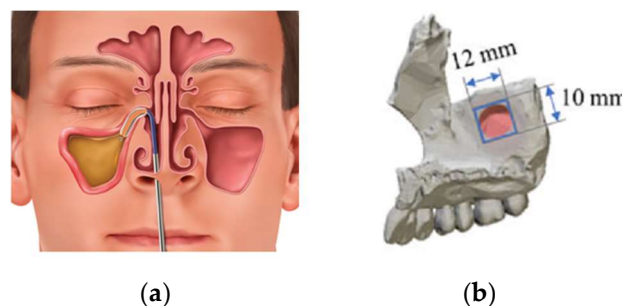


Figure 1. Maxillary sinus position: (a) front view and (b) left view.

Various techniques have been presented recently for surgical robot fault detection, identification, and tolerant control and can be divided into two main categories: a) hardware-based techniques that rely on various physical instruments installed on the surgical robot and b) software-based techniques that utilize limited equipment. Different techniques are used for software-based fault detection, estimation, and identification, such as model-reference techniques [11,12], signal-based methods [13,14], knowledge-based algorithms [15–17], and hybrid methods [18–20]. Hybrid fault detection, estimation, and identification algorithms are used to design a stable and reliable technique by employing multiple methods. Different techniques have been used for hybrid methods [18–20]. In this study, the hybrid method is designed based on three different algorithms: (a) signal-based method, (b) model-reference technique, and (c) knowledge-based algorithm. Signal-based and knowledge-based methods are used for system (surgical robotic system for the sinus) modeling based on torque and pose (position and orientation) data. A model reference technique is used to design a robust feedback linearization observer based on the variable structure technique for fault detection, estimation, and identification. A knowledge-based algorithm is used to design a Takagi–Sugeno (T–S) fuzzy technique to improve the fault estimation accuracy in the fuzzy autoregressive with exogenous input (ARX)

Laguerre robust feedback linearization observer. The hybrid technique based on adaptive fuzzy observation-based estimation and feedback linearization control is used for fault-tolerant control.

Physical-based system modeling and signal-based methods for system estimation are the main methods used for modeling complex systems such as surgical robots for the sinus. Apart from the reliability of physical-based modeling of a surgical robot for the sinus, this technique has drawbacks in highly uncertain (faulty) conditions. System estimation and identification techniques such as ARX, autoregressive moving average with external input (ARMAX), orthonormal function bases (OFB), and generalized orthonormal bases (GOB) methods have been used for system estimation in various systems. Independence of the system time delay and reduction of the number of parameters are the main advantages of orthonormal techniques such as OFB and GOB with respect to classical system modeling such as ARX and ARMAX techniques. Apart from the advantages of orthonormal techniques compared to classical algorithms, these techniques have two difficulties, calculating the optimal orthonormal values and the number of restrictions in decoupled systems. To address these issues, the ARX-Laguerre technique was presented in a number of reports [21–23]. In real world applications, the impact of noise plays a significant role in accurate system estimation. To circumvent these challenges, the fuzzy ARX-Laguerre technique is presented in this research.

Linear-based observation techniques and nonlinear-based observation algorithms are the main techniques used to design observation systems [22–25]. Linear observation systems such as proportional integral (PI) controllers have been applied in several systems for control and fault diagnosis, but their effectiveness in the presence of uncertainties is the main restriction of these algorithms [26]. To circumvent this restriction, nonlinear-based observation techniques such as variable structure techniques [22,27], feedback linearization methods [26], and fuzzy algorithms have been recommended [28–30]. Despite the advantages of nonlinear observers, a feedback linearization observer has the challenge of limited robustness [26], a variable structure observer has the limitation of chattering in uncertain conditions [22], and fuzzy logic observers have the challenge of reliability and predefinition of fuzzy gain updating factors [31] for fault detection, estimation, and identification. Consequently, a hybrid algorithm is suitable for fault detection, fault estimation, and fault identification for a surgical robot for the sinus.

Linear- and nonlinear-based fault-tolerant control techniques are the main algorithms for reducing or eliminating the effects of faults in a surgical robot for the sinus. Linear-based fault-tolerant control techniques have two main drawbacks: (a) coupling effects and (b) increase in gear ratio [32]. However, several techniques have been introduced as nonlinear-based fault-tolerant algorithms. This technique is divided into three main categories: (a) model-based algorithms, (b) knowledge-based techniques, and (c) hybrid-based fault-tolerant control methods [32]. Model-based and knowledge-based fault-tolerant control techniques have various positive points, but these techniques face a large challenge in the unlimited level of a faulty signal [18,32]. Hybrid techniques for fault-tolerant algorithms are used to address this issue [33]. The feedback linearization algorithm can be a good candidate for a fault-tolerant control algorithm, but it must be robust. To improve robustness, the proposed observation-based feedback linearization controller is the best candidate. To increase accuracy, performance, and reliability, an adaptive, fuzzy observation-based feedback linearization fault-tolerant control algorithm is suitable for manipulators for a surgical robot for the sinus.

Figure 2 shows the block diagram of the proposed algorithm for fault detection, estimation, identification, and fault-tolerant control. The proposed adaptive ARX-Laguerre T-S fuzzy robust feedback linearization observer has the following steps: (1) modeling the surgical robot for the sinus based on the ARX method; (2) modifying the performance of the ARX technique based on an orthonormal function and designing the ARX-Laguerre method; (3) improving the accuracy of the ARX-Laguerre technique based on the fuzzy logic algorithm and designing a fuzzy ARX-Laguerre system model; (4) designing a high-performance nonlinear observer based on the fuzzy ARX-Laguerre feedback linearization observation technique; (5) improving the robustness of the fuzzy ARX-Laguerre feedback linearization observer based on the variable structure algorithm; (6) improving the performance of

faulty signal estimation based on the T-S fuzzy algorithm and designing a fuzzy ARX-Laguerre T-S fuzzy robust feedback linearization observer; (7) creating a residual generation and a threshold process for fault detection and identification; (8) detecting, estimating, and identifying faults; (9) reducing the fault effect in the surgical robot for the sinus based on a feedback linearization algorithm and improving the accuracy of the fault-tolerant control using the proposed observation algorithm; and (10) tuning the feedback linearization coefficients in the various conditions and online tuning for increasing the reliability and accuracy in the proposed observation-based feedback linearization fault-tolerant control using an adaptive method.

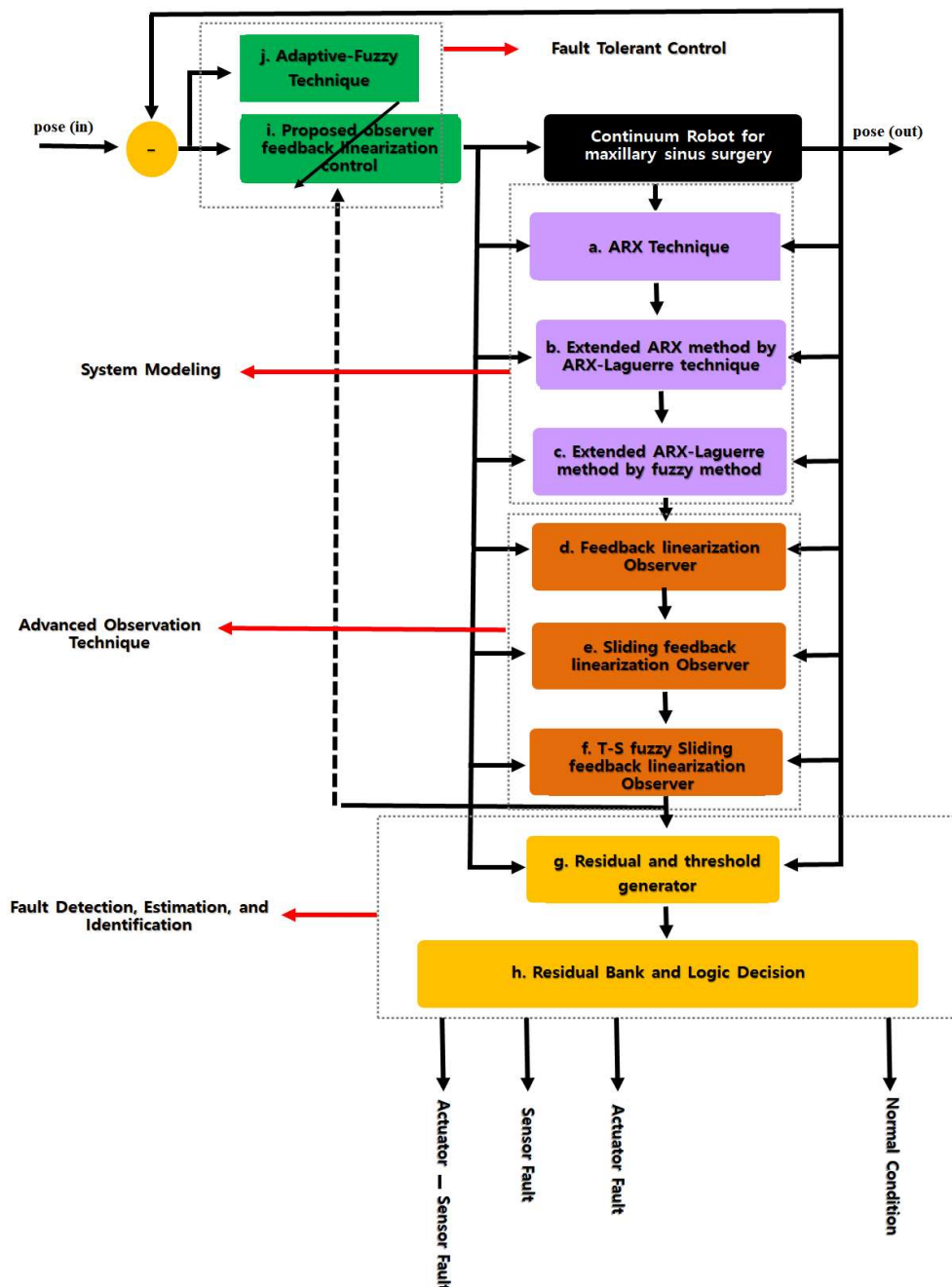


Figure 2. The proposed algorithm for fault detection, estimation, identification, and tolerant control of a maxillary sinus continuum robot surgery.

This paper introduces three different problems and the solutions to solve these problems.

Problem 1. *The main idea of the fuzzy observation-based technique for fault detection, estimation, and isolation is system modeling. Which types of system modeling are represented in this paper?*

Solution 1. *In the first step, the ARX technique is introduced to system modeling. To improve the robustness and reduce the effect of the noise, the Laguerre technique is used in the ARX technique as a ARX-Laguerre method. To reduce error of system estimation, a fuzzy ARX-Laguerre technique is performed for modeling of robotic maxillary sinus surgery (Section 2.2).*

Problem 2. *Another contribution of this paper is the design of robust and reliable technique for fault detection, estimation, and isolation. Which techniques are used in this paper?*

Solution 2. *In this study, a feedback linearization observer is used for fault estimation. To improve the robustness of the feedback linearization observer, a variable structure algorithm is employed in the next step. To modify the fault estimation accuracy in the robust feedback linearization observer, the fuzzy technique is presented in the third step (Section 3.1). To improve the fault detection and isolation, robust residual signal and threshold value are generated, compared, and classified (Section 3.2).*

Problem 3. *To reduce the effect of a fault in the robot surgery, which techniques are employed in this study?*

Solution 3. *In this study, the main idea of the fault-tolerant controller is feedback linearization control. The proposed observation technique is applied to this controller to improve the power of fault reduction. To improve the robustness in uncertain and noisy condition, a fuzzy adaptive technique is applied to the robust observation-based feedback linearization controller (Section 3.3).*

The rest of this research paper is organized as follows. In Section 2, the surgical robot for maxillary sinus surgery is modeled based on the fuzzy ARX-Laguerre procedure. The proposed adaptive fuzzy ARX-Laguerre T-S fuzzy robust feedback linearization observation for surgical robot fault detection, estimation, identification, and tolerant control are presented in Section 3. Section 3 includes three main steps. In the first step, the fuzzy ARX-Laguerre T-S fuzzy robust feedback linearization observer based on a variable structure algorithm is utilized. In the second step, fault detection, estimation, and identification are proposed. For the fault-tolerant algorithm, an adaptive fuzzy advanced observation-based feedback linearization algorithm is recommended in the third step. In Section 4, fault detection, estimation, identification, and tolerant control results for the surgical robot for maxillary sinus surgery are analyzed. Finally, the conclusions are provided in the last section.

2. Surgical Robot Modeling

Continuum robots have a biologically inspired form characterized by flexible backbones and high degree-of-freedom structures [34]. These robots have the ability to move, grasp, and manipulate into tight and congested spaces. Hence, these robots have potential applications in whole-arm grasping and manipulation in unstructured environments such as those of surgery [3]. The system information is listed in Table 1. The bending robotic system is composed of a continuum module, system drives, and control unit. The backbone of the flexible part is obtained using a superelastic NiTiNo1 tube because of its large elastic deformation, long life span, and high performance. As a result, the manipulator is safe for surgery. Figure 3 illustrates the continuum module of a surgical robot for the sinus. Figure 3a illustrates the continuum joints with four holes for NiTiNo1 tube with cable (gripper) and cable (deflection). These joints are used to improve structural stability. The joints are made of stainless steel and the manipulator consists of 17 joints and each joint can be tiled up by about 30°. Based on Figure 3b, these joints are connected by NiTiNo1 tubes and cables. Regarding Figure 3c, these cables are used to control the scissor. To improve the operational space for the sinus robot, it is designed with the rotation and translation space by spherical joints. The rotational space is used to activate the end-effector to reach the maxillary sinus and the translation space is used to reach the front and back of the maxillary sinus. The system drives are used to activate the rotational and translational motion

and the controllers are used to control of rotational, translational, deflection, and gripper (four degrees of freedom (4-DOF)) for bent to into maxillary sinus for surgical tasks [3].

Table 1. Specifications of a continuum sinus robot [3].

Part	Quantity	Description
Manipulator	Degrees of freedom	4
Continuum module	Diameter	4 [mm]
	Number of joints	17
	Maximum bending angle	270°
	Length of continuum module	30 [mm]
	Diameter of holes	0.6 [mm]
	Minimum radius of curvature	5.8 [mm]
	Radius of curvature at 180°	10 [mm]
Grippers	Length	10 [mm]
Cables (gripper)	Diameter	0.2 [mm]
	Material	Stainless Steel
Cables (deflection)	Diameter	0.36 [mm]
	Material	Stainless Steel
NiTiNo1 tube	Outer diameter	0.508 [mm]
	Inner diameter	0.305 [mm]

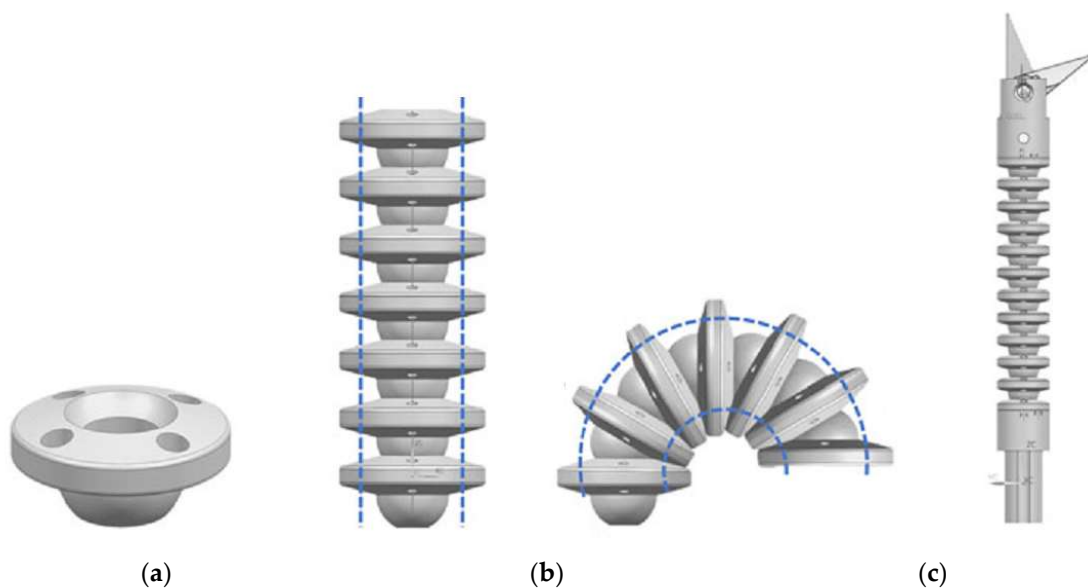


Figure 3. Continuum module of a surgical robot for the sinus: (a) continuum joint, (b) motion schematic, and (c) structure.

2.1. Surgical Robot Kinematics and Dynamics

As shown in Figure 3, a surgical robot for the sinus has two segments and two deflection stages (DS). Figure 4 shows that the proximal segment (PS) consists of areas II and III, which include seven joints, and the distal segment comprises 10 joints for areas I and IV. To analyze the continuum surgical robot for sinus deflection shown in Figure 4, the D-H conventions are presented in Table 2.

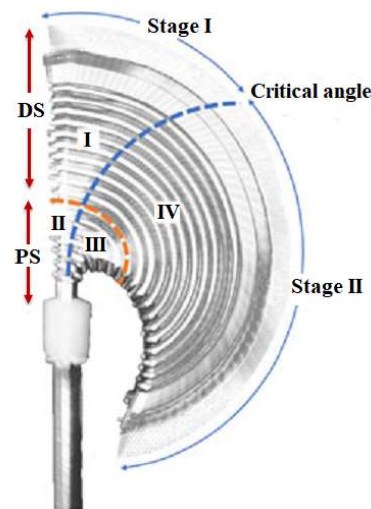


Figure 4. Four areas of deflection for sinus surgical continuum robot.

Table 2. D-H parameters of a continuum surgical robot: stage I ($\theta \leq 90^\circ$) and stage II ($\theta \geq 90^\circ$).

Link	α	a	d	θ	State
1	0	a_1	d_1	0	$\theta \leq 90^\circ$
2	-90°	0	d_2	ϕ	$\theta \leq 90^\circ$
3	90°	0	0	θ_3	$\theta \leq 90^\circ$
4	-90°	0	d_4	0	$\theta \leq 90^\circ$
5	90°	0	0	θ_5	$\theta \leq 90^\circ$
6	0	0	d_5	0	$\theta \leq 90^\circ$
7	0	0	d_6	0	$\theta \leq 90^\circ$
8	0	a_1	d_1	0	$\theta \geq 90^\circ$
9	-90°	0	d_2	-90°	$\theta \geq 90^\circ$
10	90°	0	0	90°	$\theta \geq 90^\circ$
11	-90°	0	d_4	-90°	$\theta \geq 90^\circ$
12	90°	0	0	90°	$\theta \geq 90^\circ$
13	-90°	0	0	-90°	$\theta \geq 90^\circ$
14	90°	0	0	90°	$\theta \geq 90^\circ$
15	-90°	0	d_8	-90°	$\theta \geq 90^\circ$
16	90°	0	0	90°	$\theta \geq 90^\circ$
17	0	0	d_{10}	0	$\theta \geq 90^\circ$

The translation matrix is defined by the following equation:

$${}^i T = \begin{bmatrix} \cos \theta_i & -\sin \theta_i & 0 & a_{i-1} \\ \sin \theta_i \cos \alpha_{i-1} & \cos \theta_i \cos \alpha_{i-1} & -\sin \alpha_{i-1} & -\sin \alpha_{i-1} d_i \\ \sin \theta_i \sin \alpha_{i-1} & \cos \theta_i \sin \alpha_{i-1} & \cos \alpha_{i-1} & \cos \alpha_{i-1} d_i \\ 0 & 0 & 0 & 1 \end{bmatrix} \tag{1}$$

Here, ${}^i T$, a_i , α_i , d_i and θ_i are the transformation matrix for each link, the distance from \hat{Z}_i to \hat{Z}_{i+1} measured along \hat{X}_i , the angle from \hat{Z}_i to \hat{Z}_{i+1} measured about \hat{X}_i , the distance from \hat{X}_{i-1} to \hat{X}_i measured along \hat{Z}_i , and the angle from \hat{X}_{i-1} to \hat{X}_i measured about \hat{Z}_i , respectively. Based on Equation (1), the forward kinematics is represented by Equation (2).

$$FK = {}^0 T_{17} = {}^0 T_1 T_2 T_3 T_4 T_5 T_6 T_7 T_8 T_9 T_{10} T_{11} T_{12} T_{13} T_{14} T_{15} T_{16} T_{17} \tag{2}$$

A slave robot manipulator to drive a surgical continuum robot has 4-DOF, is serial linked, and is a coupling effects system. The configurations for continuum sinus surgery with the master robot are

illustrated in Figure 5. As shown in Figure 5, the master manipulator is used for input control, and four controllers are designed to control the four motors located in the slave manipulator. As shown in Figure 6, these motors are used to actuate the translation, rotation, deflection, and gripper of the surgical robot for the sinus.

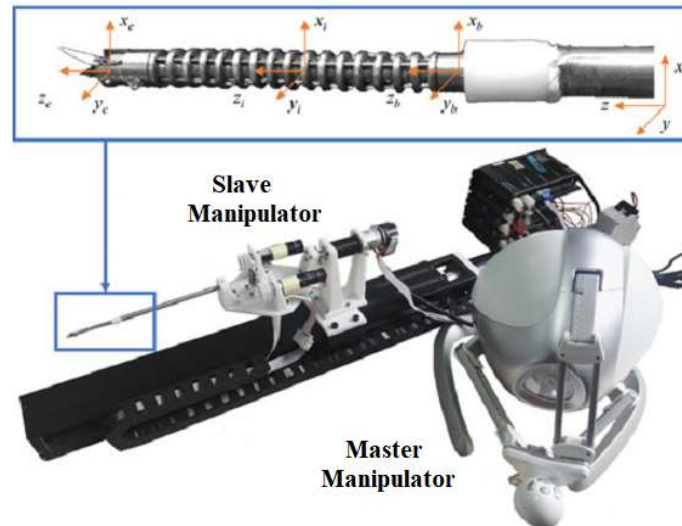


Figure 5. Surgical sinus robot manipulator.

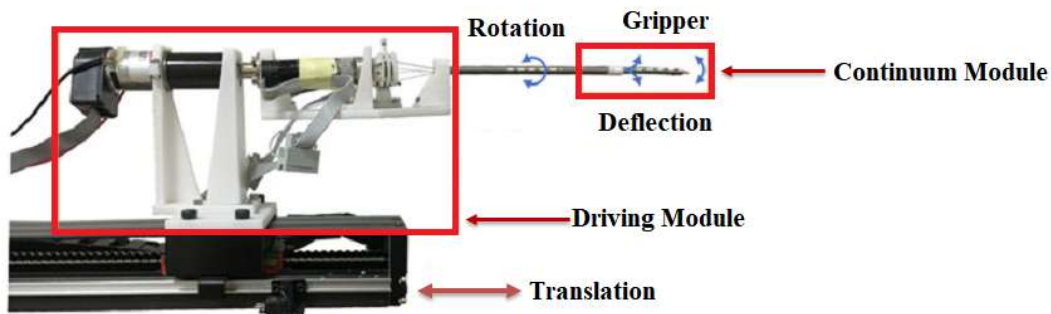


Figure 6. Fundamental drivers of the slave manipulator.

The dynamic formulation of the surgical robot for the sinus is represented by Equation (3) [34–36].

$$F_c \tau = I(q) \ddot{q} + N(q, \dot{q}) + G(q) + \delta, \tag{3}$$

where F_c , τ , $I(q)$, $N(q, \dot{q})$, $G(q)$, and δ are the force coefficient matrix, inertial matrix, coefficients of the first-order generalized coordinate matrix, gravity, and faults and uncertainties, respectively. The force coefficient matrix transforms the input forces to the generalized forces and torques in the system. The inertia matrix is composed of four block matrices. The block matrices that correspond to pure linear accelerations and pure angular accelerations in the system are symmetrical. The matrix $N(q)$ contains coefficients of the first order derivatives of the generalized co-ordinates. Since the system is nonlinear, many elements of $N(q)$ contain first order derivatives of the generalized co-ordinates. The remaining terms in the dynamic equations resulting from gravitational potential energies and spring energies are collected in this matrix. Therefore, the joint position is represented by Equation (4).

$$\iint \ddot{q} = \iint I(q)^{-1} \times (F_c \tau - N(q, \dot{q}) - G(q)) + \delta \tag{4}$$

Hence, the state-space equation is introduced as follows [14]:

$$\begin{cases} X_{q,F_c\tau}(k+1) = I(q)^{-1}(X_{q,F_c\tau}U_{F_c\tau}(k) + \xi(X_{q,F_c\tau}) + \delta(k) \\ Y_q(k+1) = (\kappa)^T X_{q,F_c\tau} \end{cases} \quad (5)$$

Here, $\xi(X_{q,F_c\tau}) = (N(q, \dot{q}) + G(q))$. The $X_{q,F_c\tau}(k)$, $U_{F_c\tau}(k)$, $Y_q(k)$, and κ are the state function, state input, state output, and Fourier coefficient, respectively. To design an observation-based fault diagnosis and fault-tolerant control, modeling of the surgical robot for the sinus is the first step.

2.2. Fuzzy Auto Regressive with Exogenous Input (ARX) Laguerre System Modeling

Based on Figure 2, the proposed system modeling has three main steps: (a) ARX technique, (b) improve the robustness of the ARX technique by the orthonormal method and design of the ARX-Laguerre method, and (c) improve the accuracy of system estimation based on the fuzzy ARX-Laguerre technique. An extensive variety of sinus surgery continuum robots based on the ARX method is represented by the following equation [37]:

$$W(k) + \lambda_{W_1}W(k-1) + \lambda_{W_2}W(k-2) + \dots + \lambda_{W_W}W(k-n_W) = \lambda_{H_1}H(k-1) + \lambda_{H_2}H(k-2) + \dots + \lambda_{H_H}H(k-n_H) + e(k) \quad (6)$$

Therefore, the future output can be predicted by observation parameters based on Equation (7).

$$W(k) = -\lambda_{W_1}W(k-1) - \lambda_{W_2}W(k-2) - \dots - \lambda_{W_W}W(k-n_W) + \lambda_{H_1}H(k-1) + \lambda_{H_2}H(k-2) + \dots + \lambda_{H_H}H(k-n_H) + e(k) \quad (7)$$

where $(W(k-n_W), H(k-n_H)), W(k), H(k), (\lambda_W, \lambda_H)$, and $e(k)$ are system lag, output, input, coefficients, and zero-mean noise, respectively. Building on Equation 7, the state-space ARX modeling is represented by Equation (8).

$$\begin{cases} W(k) = -\varepsilon(k).\psi + e(k) \\ \psi = [\lambda_{W_1} \dots \lambda_{W_W} \lambda_{H_1} \dots \lambda_{H_H}] \\ \varepsilon = [-W(k-1) \dots -W(k-n_W) \ H(k-1) \dots \ H(k-n_H)] \end{cases} \quad (8)$$

Here, ε and ψ are regressor variables of the ARX system modeling and the coefficient matrix, respectively. Thus, Equation (8) represents the ARX estimation technique.

$$W(k) = \hat{\phi}[W(k-1), W(k-2), \dots, W(k-n_W), H(k-1), H(k-2), \dots, H(k-n_H)], \quad (9)$$

$$\begin{aligned} \hat{\phi} &= \arg \min_{\hat{\phi}} \{f(\hat{\phi}, \psi)\} \\ f(\hat{\phi}, \psi) &= \frac{1}{k} \sum_0^k (W(k) - \varepsilon(k)\psi)^2 \end{aligned} \quad (10)$$

Therefore, the state-space ARX system modeling is represented by the following equation.

$$\begin{cases} X_{q,F_c\tau}(k+1) = \alpha_X X_{q,F_c\tau} + \alpha_U U_{F_c\tau}(k) + \delta(k) \\ Y_q(k+1) = (\kappa)^T X_{q,F_c\tau} \end{cases} \quad (11)$$

Here, (α_X, α_U) are coefficients. To improve the accuracy and reduce the system estimation order, the ARX-Laguerre technique for modeling the surgical robot for the sinus is represented by the following equation [18,21].

$$Y_q(k) = \sum_0^{i_Y} \alpha_{n,Y} \left(\sum_{j=1}^{\infty} \lambda_Y * Y_q(k) \right) \cdot \chi_{n,Y}(k) + \sum_0^{i_U} \alpha_{n,U} \left(\sum_{j=1}^{\infty} \lambda_U * U(k) \right) \cdot \chi_{n,U}(k), \quad (12)$$

where $(\alpha_{n,Y} \& \alpha_{n,U}), (i_Y, i_U), (\lambda_Y, \lambda_U), *, \chi_{n,Y(k)}$ and $\chi_{n,U(k)}$ are the Fourier coefficients, the robot manipulator order, the function of the Laguerre orthonormal, the product of the convolution, the filter system output, and the filter system input, respectively. Figure 7 illustrates the block diagram of the ARX-Laguerre algorithm. Here, $\phi_{o1} = \frac{\sqrt{1-\zeta_a}}{Z-\zeta_a}, \phi_{o2} = \phi_{on} = \frac{1-\zeta_a z}{Z-\zeta_a}, \phi_{i1} = \frac{\sqrt{1-\zeta_b}}{Z-\zeta_b}, \phi_{i2} = \phi_{in} = \frac{1-\zeta_b z}{Z-\zeta_b}, \kappa = [G_{0,a}, \dots, G_{n,a}, G_{0,b}, \dots, G_{n,b}]$, and (ζ_a, ζ_b) is the orthonormal basis. Therefore, the state-space ARX-Laguerre surgical robot estimation is represented by the following equation.

$$\begin{cases} X_{q,Fc\tau}(k+1) = [\alpha_X X_{q,Fc\tau} + \alpha_U U_{Fc\tau}(k) + \alpha_Y Y_q(k)] + \delta(k) \\ Y_q(k+1) = (\kappa)^T X_{q,Fc\tau} \end{cases} \quad (13)$$

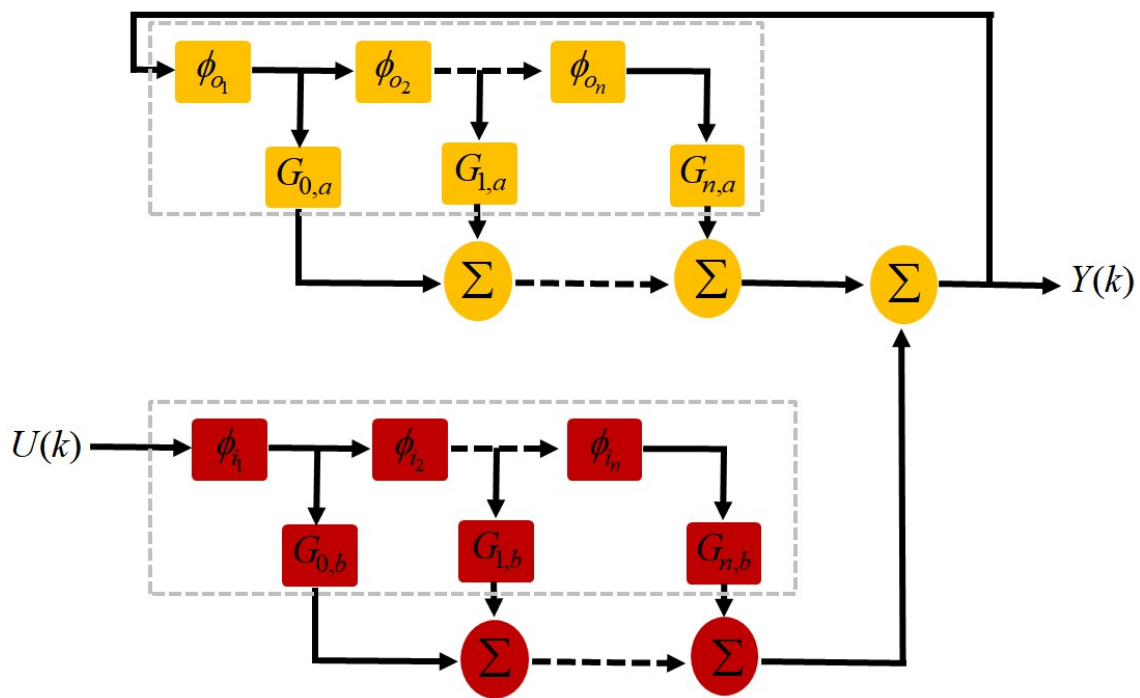


Figure 7. Auto regressive with exogenous input (ARX) Laguerre method for modeling the surgical robot for the sinus manipulator.

In this research, to modify the accuracy of the ARX-Laguerre method, a fuzzy logic technique is recommended. Based on the bounds of the uncertainties and faults, the primary objective is to present a systematic fuzzy algorithm for modeling the multi-input-multi-output (MIMO) systems in the presence of unknown parameters. Based on the fuzzy algorithm, this technique consists of the following parts: fuzzification, an IF-THEN rule, a reasoning mechanism, and defuzzification. The primary challenge of system modeling based on the fuzzy algorithm is improving the performance of the knowledge base and inference parts. The fuzzy ARX-Laguerre system estimation is defined based on the following equation:

$$W_{fuzzy}(k) = f_{fuzzy}[W(k-1), W(k-2), \dots, W(k-n_W), H(k-1), H(k-2), \dots, H(k-n_H)], \quad (14)$$

where f_{fuzzy} is a fuzzy function for system estimation. The fuzzy IF-THEN rule is defined as follows [28]:

$$\text{Rule (N) : If } e_m \text{ is } H_e^m \text{ and } \dot{e}_m \text{ is } H_{\dot{e}}^m \text{ then } f_{fuzzy} \text{ is } H_{fuzzy}^m \quad (15)$$

where $e_m, (H_e^m, H_{\dot{e}}^m, H_{fuzzy}^m)$, and \dot{e}_m are the estimation error, the fuzzy sets, and the estimation change of error, respectively. The fuzzy membership functions for e_m in the interval of $[-0.1, 0.1]$ are Gaussian,

and the fuzzy sets are defined as negative big (NB), negative small (NS), zero (Z), positive small (PS), and positive big (PB). The fuzzy membership functions for \dot{e}_m in the interval of $[-1, 1]$ are Gaussian, and the fuzzy sets are defined as NB, NS, Z, PS, and PB. The fuzzy membership functions for f_{fuzzy} in the interval of $[-10, 10]$ are Gaussian, and the fuzzy sets are defined as NB, NS, Z, PS, and PB. Thus, the state-space fuzzy ARX-Laguerre estimation for the surgical robot for the sinus is represented by:

$$\begin{cases} X_{q,Fc\tau}(k+1) = [\alpha_X X_{q,Fc\tau} + \alpha_U U_{Fc\tau}(k) + \alpha_Y Y_q(k) + \alpha_F f_{fuzzy}] + \delta(k) \\ Y_q(k+1) = (\kappa)^T X_{q,Fc\tau} \end{cases} \quad (16)$$

where $(\alpha_X, \alpha_U, \alpha_Y, \alpha_F)$ are coefficients. The rule table of the fuzzy ARX-Laguerre algorithm is shown in Table 3.

Table 3. Fuzzy rule table for the fuzzy ARX-Laguerre surgical robot for the sinus estimation algorithm.

		Change of Error (de)				
		NB	NS	Z	PS	PB
Error (e)	NB	PB	PB	PB	PS	Z
	NS	PB	PB	PS	Z	NS
	Z	PB	PS	Z	NS	NB
	PS	PS	Z	NS	NB	NB
	PB	Z	NS	NB	NB	NB

Figures 8 and 9 illustrate the estimation accuracy and errors for the normal and abnormal conditions based on the ARX method, the ARX-Laguerre technique, and the fuzzy ARX-Laguerre algorithm. According to these figures, the estimation accuracy of the fuzzy ARX-Laguerre technique is higher than those of the ARX and ARX-Laguerre techniques, and the error rate in the fuzzy ARX-Laguerre estimation technique is close to zero under normal and abnormal conditions.

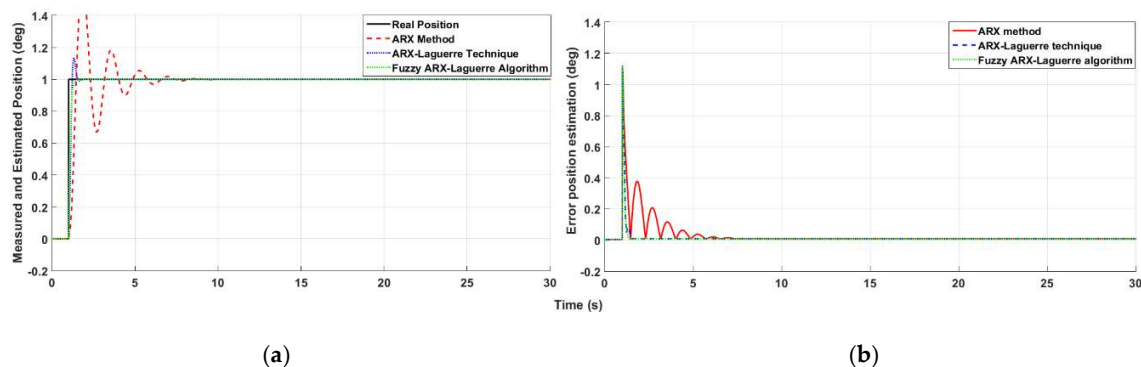


Figure 8. Proposed fuzzy ARX-Laguerre method, ARX-Laguerre technique, and ARX algorithm for position estimation of the surgical robot for the sinus under normal conditions. (a) Measured and estimated position. (b) Error of estimated position.

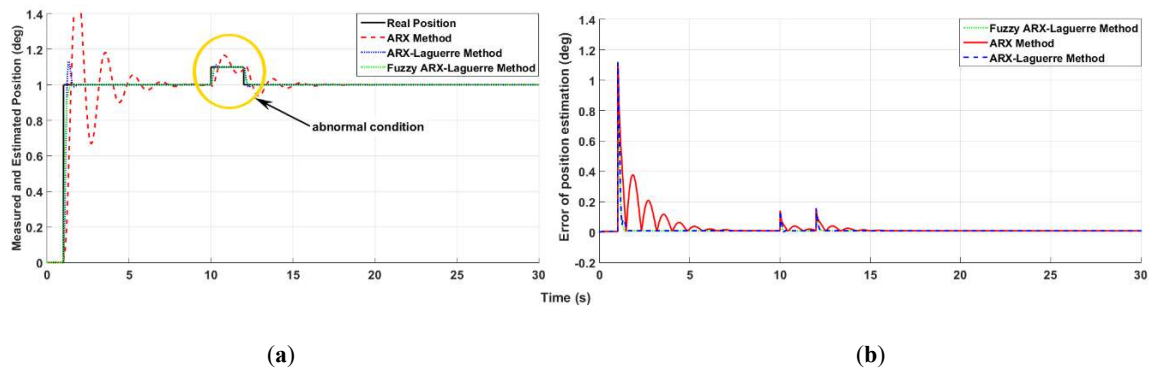


Figure 9. Proposed fuzzy ARX-Laguerre method, ARX-Laguerre technique, and ARX algorithm position estimation of the surgical robot for the sinus under abnormal conditions. (a) Measured and estimated position. (b) Error of estimated position.

3. Proposed Method for Fault Estimation, Detection, Identification and Tolerant Control

Based on the algorithm shown in Figure 2, the surgical robot for the sinus was modeled using the fuzzy ARX-Laguerre method. After modeling the surgical robot for the sinus with the fuzzy ARX-Laguerre technique, the advanced intelligent nonlinear observer was designed. In the next step, fault detection, estimation, and identification were analyzed. In the last step, fault-tolerant control was designed to eliminate or reduce the effect of faults of the surgical robot for the sinus based on the proposed adaptive fuzzy observer feedback linearization controller.

3.1. Takagi–Sugeno (T–S) Fuzzy Advanced Observer

Following the abbreviations shown in Figure 2, the fuzzy ARX-Laguerre T–S fuzzy robust feedback linearization observer designed in this section comprises three main blocks: (d) the fuzzy ARX-Laguerre feedback linearization observer, (e) improvement of the robustness and estimation performance based on the fuzzy ARX-Laguerre robust (variable structure) feedback linearization observer algorithm, and (f) reduction of the estimation error of the fuzzy ARX-Laguerre robust feedback linearization observer based on the T–S fuzzy algorithm and formulation of the fuzzy ARX-Laguerre T–S fuzzy robust feedback linearization technique. The feedback linearization observer offers a non-linear model-reference approach to find an accurate system and fault estimation. Based on Equation (16), the fuzzy ARX-Laguerre feedback linearization observer is proposed for a surgical robot for the sinus based on the following Equation (26):

$$\begin{cases} \hat{X}_{q,F_c\tau}(FLO)(k+1) = [\alpha_X \hat{X}_{q,F_c\tau}(FLO) + \alpha_U U_{F_c\tau}(k) + \alpha_Y \hat{Y}_{q(FLO)}(k) + \alpha_F \hat{f}_{fuzzy}(FLO)] \\ + \hat{\delta}_{(FLO)}(k) + \alpha_P (Y_q(k) - \hat{Y}_{q(FLO)}(k)) + f(\hat{X}_{q,F_c\tau}(FLO), U) + I^{-1}(\alpha_P (Y_q(k) - \hat{Y}_{q(FLO)}(k))) \\ \hat{Y}_{q(FLO)}(k+1) = (\kappa)^T \hat{X}_{q,F_c\tau}(FLO)(k) \end{cases} \quad (17)$$

where $f(\hat{X}_{q,F_c\tau}(FLO), U) = I^{-1}[F_c\tau - N(q, \dot{q}) - G(q)]$. Here, $\hat{X}_{q,F_c\tau}(FLO)(k)$, $\hat{Y}_{q(FLO)}(k)$, $\hat{f}_{fuzzy}(FLO)$, $\hat{\delta}_{(FLO)}(k)$, and α_p are the state estimation, output estimation, fuzzy estimation function, fault estimation, and a coefficient, respectively. Except for α_p , all are based on the fuzzy ARX-Laguerre feedback linearization observer. The fault is estimated in the fuzzy ARX-Laguerre feedback linearization observer based on Equation (18).

$$\hat{\delta}_{(FLO)}(k+1) = I^{-1}(\hat{\delta}_{(FLO)}(k) + \alpha_P (Y_q(k) - \hat{Y}_{q(FLO)}(k))) \quad (18)$$

The state and fault estimation errors in the fuzzy ARX-Laguerre feedback linearization observer are represented by Equation (19).

$$\begin{cases} \tilde{X}_{q,F_c\tau}(FLO)(k) = X_{q,F_c\tau}(k) - \hat{X}_{q,F_c\tau}(FLO)(k) \\ \tilde{\delta}_{(FLO)}(k) = \delta(k) - \hat{\delta}_{(FLO)}(k) \end{cases} \quad (19)$$

Here, $\widetilde{X}_{q,F_c\tau(RFLO)}(k)$ and $\widetilde{\delta}_{(RFLO)}(k)$ are the state estimation error and fault estimation error, respectively. Both are based on the fuzzy ARX-Laguerre feedback linearization observer. To improve the robustness of the fuzzy ARX-Laguerre feedback linearization observer, the fuzzy ARX-Laguerre extended feedback linearization observer based on the variable structure technique is recommended. Based on previous work [18,23,26,27], the variable structure technique is a robust, stable, and reliable method for fault estimation. Thus, to improve the reliability, robustness, and estimation accuracy, the fuzzy ARX-Laguerre variable structure feedback linearization observer is a respectable candidate. The variable structure fault estimation technique is represented by Equation (20).

$$\dot{\delta}_{VSO}(k+1) = (\kappa_{VSO}) \times \text{sgn}(Y_q(k) - \hat{Y}_{q(RFLO)}(k)) \tag{20}$$

Based on Equations (17), (18), and (20), the state-space and fault estimation of the fuzzy ARX-Laguerre robust (variable structure) feedback linearization observer are represented by Equations (21) and (22).

$$\begin{cases} \hat{X}_{q,F_c\tau(RFLO)}(k+1) = [\alpha_X \hat{X}_{q,F_c\tau(RFLO)} + \alpha_U U_{F_c\tau}(k) + \alpha_Y \hat{Y}_{q(RFLO)}(k) + \alpha_F \hat{f}_{fuzzy(RFLO)}] \\ + \hat{\delta}_{(RFLO)}(k) + \alpha_P(Y_q(k) - \hat{Y}_{q(RFLO)}(k)) + f(\hat{X}_{q,F_c\tau(RFLO)}, U) + I^{-1}(\alpha_P(Y_q(k) - \hat{Y}_{q(RFLO)}(k))) \\ \hat{Y}_{q(RFLO)}(k+1) = (\kappa)^T \hat{X}_{q,F_c\tau(RFLO)}(k) \end{cases} \tag{21}$$

$$\hat{\delta}_{(RFLO)}(k+1) = I^{-1}(\hat{\delta}_{(RFLO)}(k) + \alpha_P(Y_q(k) - \hat{Y}_{q(RFLO)}(k))) + (\kappa_{VSO}) \| (Y_q(k) - \hat{Y}_{q(RFLO)}(k)) \|^{0.5} \times \text{sgn}(Y_q(k) - \hat{Y}_{q(RFLO)}(k)) - \hat{\delta}_{(RFLO)}(k) \tag{22}$$

The state and fault estimation errors in the fuzzy ARX-Laguerre robust feedback linearization observer based on the variable structure algorithm are represented by Equation (23).

$$\begin{cases} \widetilde{X}_{q,F_c\tau(RFLO)}(k) = X_{q,F_c\tau}(k) - \hat{X}_{q,F_c\tau(RFLO)}(k) \\ \widetilde{\delta}_{(RFLO)}(k) = \delta(k) - \hat{\delta}_{(RFLO)}(k) \end{cases}, \tag{23}$$

where $\hat{X}_{q,F_c\tau(RFLO)}(k)$, $\hat{Y}_{q(RFLO)}(k)$, $\hat{\delta}_{(RFLO)}(k)$, κ_{VSO} , $\widetilde{X}_{q,F_c\tau(RFLO)}(k)$, and $\widetilde{\delta}_{(RFLO)}(k)$ are state estimation, the fuzzy ARX-Laguerre robust feedback linearization output estimation, fault estimation, the observer coefficient, state estimation error, and fault estimation error, respectively, all based on fuzzy ARX-Laguerre robust feedback linearization. The fuzzy ARX-Laguerre robust feedback linearization observer based on the variable structure technique amended the robustness of the fuzzy ARX-Laguerre feedback linearization observer; however, to improve fault estimation accuracy, the fuzzy ARX-Laguerre T-S fuzzy robust feedback linearization technique is recommended. The T-S fuzzy observer is represented by the following function [28].

$$\text{IF } r_a(k) \text{ is } TH_a \text{ and } r_s(k) \text{ is } TH_s \text{ THEN } \hat{\delta}_{fuzzy}(k+1) = \hat{\delta}_{fuzzy}(k) + \alpha_{fuzzy}(Y_q(k) - \hat{Y}_q(k)), \tag{24}$$

Here, $r_a(k)$, $r_s(k)$, (TH_a, TH_s) , $\hat{\delta}_{fuzzy}(k)$, and α_{fuzzy} are the residual signal for the actuator fault, residual signal for the sensor fault, threshold values for the actuator and sensor faults, faulty signal estimator based on the T-S fuzzy algorithm, and the fuzzy coefficient, respectively. Based on Equation (24), the rule base for the T-S fuzzy technique to estimate the fault is represented by the following Equation.

$$\hat{\delta}_{fuzzy} : \begin{cases} \text{IF } r_a(k) \text{ is } TH_a \text{ and } r_s(k) \cong 0 \text{ THEN } \hat{\delta}_{fuzzy}(k+1) = \hat{\delta}_{fuzzy}(k) + \alpha_{1fuzzy}(Y_q(k) - \hat{Y}_q(k)) \\ \text{IF } r_a(k) \cong 0 \text{ and } r_s(k) \text{ is } TH_s \text{ THEN } \hat{\delta}_{fuzzy}(k+1) = \hat{\delta}_{fuzzy}(k) + \alpha_{2fuzzy}(Y_q(k) - \hat{Y}_q(k)) \\ \text{IF } r_a(k) \text{ is } TH_a \text{ and } r_s(k) \text{ is } TH_s \text{ THEN } \hat{\delta}_{fuzzy}(k+1) = \hat{\delta}_{fuzzy}(k) + \alpha_{3fuzzy}(Y_q(k) - \hat{Y}_q(k)) \end{cases} \tag{25}$$

Here, $(\alpha_{1fuzzy}, \alpha_{2fuzzy}, \alpha_{3fuzzy})$, TH_a and TH_s are fuzzy estimator coefficients for actuator fault, sensor fault, and actuator-sensor fault and actuator and sensor thresholds, respectively. Concerning

Equations (21), (22), and (25), the fuzzy ARX-Laguerre T-S fuzzy robust feedback linearization observer is represented by Equations (26) and (27).

$$\begin{cases} \hat{X}_{q,F_c\tau(p)}(k+1) = [\alpha_X \hat{X}_{q,F_c\tau(p)} + \alpha_U U_{F_c\tau}(k) + \alpha_Y \hat{Y}_{q(p)}(k) + \alpha_F \hat{f}_{fuzzy(p)}] \\ + \hat{\delta}_{(p)}(k) + \alpha_P (Y_q(k) - \hat{Y}_{q(p)}(k)) + f(\hat{X}_{q,F_c\tau(p)}, U) + I^{-1}(\alpha_P (Y_q(k) - \hat{Y}_{q(p)}(k))) \\ \hat{Y}_{q(p)}(k+1) = (\kappa)^T \hat{X}_{q,F_c\tau(p)}(k) \end{cases} \quad (26)$$

$$\begin{aligned} \hat{\delta}_{(p)}(k+1) &= I^{-1}(\hat{\delta}_{(FLO)}(k) + \alpha_P (Y_q(k) - \hat{Y}_{q(p)}(k))) + (\kappa_{VSO}) \| (Y_q(k) - \hat{Y}_{q(p)}(k)) \|^{0.5} \times \\ &\text{sgn}(Y_q(k) - \hat{Y}_{q(p)}(k)) - \hat{\delta}_{(RFLO)}(k) + \hat{\delta}_{(fuzzy)}(k) \end{aligned} \quad (27)$$

The state and fault estimation errors in the fuzzy ARX-Laguerre T-S fuzzy robust feedback linearization observer are represented by Equation (28).

$$\begin{cases} \tilde{X}_{q,F_c\tau(p)}(k) = X_{q,F_c\tau}(k) - \hat{X}_{q,F_c\tau(p)}(k) \\ \tilde{\delta}_{(p)}(k) = \delta(k) - \hat{\delta}_{(p)}(k) \end{cases}, \quad (28)$$

where $\hat{X}_{q,F_c\tau(p)}(k)$, $\hat{Y}_{q(p)}(k)$, $\hat{\delta}_{(p)}(k)$, $\tilde{X}_{q,F_c\tau(p)}(k)$, and $\tilde{\delta}_{(p)}(k)$ are the fuzzy ARX-Laguerre T-S fuzzy robust feedback linearization (proposed) observer for state estimation and the proposed observers for output estimation, fault estimation, state estimation error, and fault estimation error, respectively. Figure 10 illustrates the fault estimation and fault estimation error for the fuzzy ARX-Laguerre feedback linearization observer, fuzzy ARX-Laguerre robust feedback linearization observer based on the variable structure technique, and proposed fuzzy ARX-Laguerre fuzzy robust feedback linearization observer for normal and abnormal conditions for the surgical robot for the sinus. Regarding this figure, the fault estimation accuracy and error of fault estimation based on the proposed algorithm are more accurate than those of the fuzzy ARX-Laguerre feedback linearization observer and fuzzy ARX-Laguerre robust feedback linearization observer.

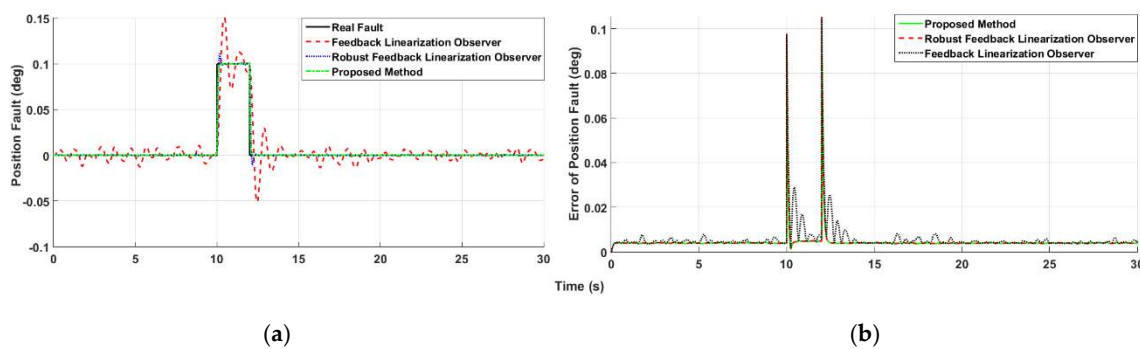


Figure 10. Results for the fuzzy ARX-Laguerre feedback linearization method, fuzzy ARX-Laguerre robust feedback linearization method, and fuzzy ARX-Laguerre T-S fuzzy robust feedback linearization method for the surgical robot for the sinus. (a) Position fault estimation accuracy. (b) Fault estimation error of position estimation.

3.2. Fault Detection, Estimation, and Identification Technique

As identified in Figure 2, the fault detection, estimation, and identification blocks have two sub-blocks: (g) residual and threshold generator and (h) residual bank and logic decision. The residual signal is generated by Equation (29).

$$r = Y_{(q)} - \hat{Y}_{q(p)} \quad (29)$$

Based on previous work [18,23,26,27], the robust sliding mode algorithm is used to generate the threshold value. The sliding mode threshold value is generated by Equation (30).

$$\begin{cases} TH_N = \alpha_N[\text{sgn}(\lambda_N \times r_N + (\frac{\lambda_N}{2})^2 \sum r_N + \dot{r}_N)] \\ TH_a = \alpha_a[\text{sgn}(\lambda_a \times r_a + (\frac{\lambda_a}{2})^2 \sum r_a + \dot{r}_a)] \\ TH_s = \alpha_s[\text{sgn}(\lambda_s \times r_s + (\frac{\lambda_s}{2})^2 \sum r_s + \dot{r}_s)] \end{cases} \quad (30)$$

Here, $TH_N, TH_a, TH_s, (\alpha_N, \alpha_a, \alpha_s, \lambda_N, \lambda_a, \lambda_s), r_N, \dot{r}_N, \sum r_N, \dot{r}_a, \sum r_a, r_s, \dot{r}_s,$ and $\sum r_s$ are the threshold value for normal condition, threshold value for actuator fault, threshold value for sensor fault, coefficients of the sliding mode algorithm in different states, residual signal for normal condition, change of residual signal for normal condition, integral of residual signal for normal condition, residual signal for actuator fault, change of residual signal for actuator fault, integral of residual signal for actuator fault, residual signal for sensor fault, change of residual signal for sensor fault, and integral of residual signal for sensor fault, respectively. Two different conditions have been defined for fault detection in the surgical robot for the sinus: (a) normal condition ($\delta(k) = 0$) and (b) abnormal condition ($\delta(k) \neq 0$). The fault detection in the manipulator of the surgical robot for the sinus is represented by Equation (31).

$$\begin{cases} \text{Normal Condition} : r(k) < TH_N \\ \text{abnormal Condition} : r(k) \geq TH_N \end{cases} \quad (31)$$

Figure 11 illustrates the fault detection for the fuzzy ARX-Laguerre feedback linearization observer, fuzzy ARX-Laguerre robust feedback linearization observer, and proposed algorithm. Based on the fuzzy ARX-Laguerre fuzzy robust feedback linearization observer, the proposed high-accuracy fault estimation technique is represented by Equation (27). Based on Equations (26)–(31), the following equation is used for fault identification for the manipulator of the surgical robot for the sinus.

$$\begin{cases} (\text{Actuator}) \text{ Fault} : (r_a(k) \geq TH_a \ \& \ TH_N \leq r_s(k) < TH_s) \\ (\text{Sensor}) \text{ Fault} : (TH_N \leq r_a(k) < TH_a \ \& \ r_s(k) \geq TH_s) \\ (\text{Sensor} - \text{Actuator}) \text{ Fault} : (r_a(k) \geq TH_a \ \& \ r_s(k) \geq TH_s) \end{cases} \quad (32)$$

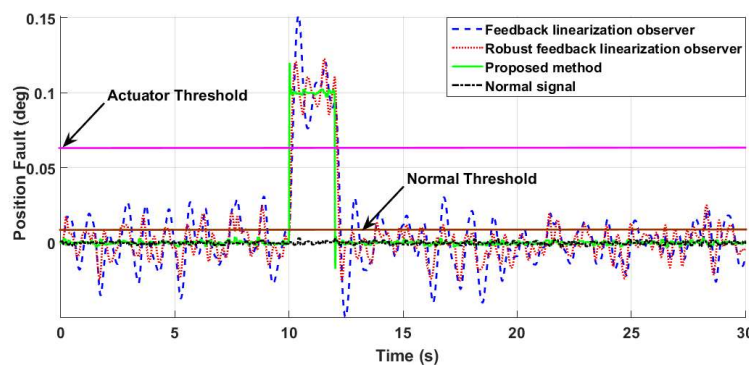


Figure 11. Fault detection for the fuzzy ARX-Laguerre feedback linearization method, the fuzzy ARX-Laguerre robust feedback linearization method, and the fuzzy ARX-Laguerre T-S fuzzy robust feedback linearization method for the surgical robot for the sinus.

Figure 12 illustrates the fault identification in the manipulator of the surgical robot for the sinus for the fuzzy ARX-Laguerre feedback linearization observer, fuzzy ARX-Laguerre robust feedback linearization observer, and the proposed algorithm. Based on fault estimation accuracy, the proposed algorithm has better performance for fault diagnosis time delay.

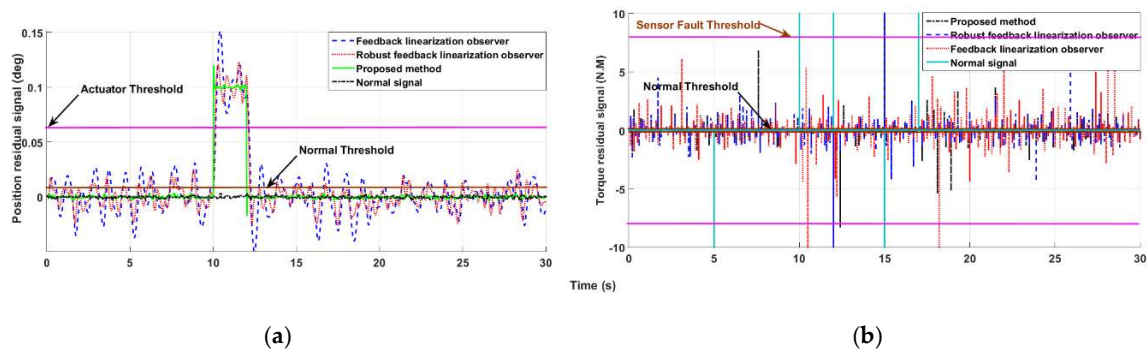


Figure 12. Actuator fault identification residual signals: (a) position and (b) torque for the fuzzy ARX-Laguerre feedback linearization method, the fuzzy ARX-Laguerre robust feedback linearization method, and the fuzzy ARX-Laguerre T-S fuzzy robust feedback linearization method for the surgical robot for the sinus.

3.3. Fault-Tolerant Control

A fault-tolerant controller is used to reduce or eliminate the effect of faults in the surgical robot for the sinus. As shown in Figure 2, the fault-tolerant control section has two main subparts: (i) proposed observation-based feedback linearization control; and (j) adaptive-fuzzy technique. The proposed observation-based feedback linearization control has two main subparts: (1) the classical feedback linearization control; and (2) the proposed observation algorithm designed in the previous section and based on the fuzzy ARX-Laguerre T-S fuzzy robust feedback linearization observer. Based on Figures 5 and 6, four PC-based controllers are designed to control four motors located in the slave manipulator. These motors are used to actuate the translation, rotation, deflection, and gripper of the surgical robot. The conventional feedback linearization fault-tolerant control is represented in the following Equation:

$$\begin{cases} \tau_{FLC}(k) = -I(q) \times (\ddot{X}_d + \alpha_p e(k) + \alpha_d \dot{e}(k) + \alpha_i \sum e(k)) + f(\hat{X}_{q,F_c\tau}(p), U) \\ e(k) = (Y_q(k) - \hat{Y}_{q(p)}(k)) \end{cases}, \quad (33)$$

Here, τ_{FLC} and $(\alpha_p, \alpha_d, \alpha_i)$ are the controller output (torque) based on the conventional feedback linearization control algorithm and controller coefficients, respectively. In addition to several positive points of classical feedback linearization control algorithm, to improve the robustness and increase the power of fault reduction, the proposed fuzzy ARX-Laguerre T-S fuzzy robust feedback linearization observer is presented. The main advantage of this part is to estimate the unmeasured variable ($\hat{X}_{q,F_c\tau}$) by observation. The proposed observer feedback linearization control is represented by the following Equation:

$$\begin{cases} \tau_{OFLC}(k) = \tau_{FLC}(k) + \hat{Y}_{q(p)}(k) \\ \hat{Y}_{q(p)}(k+1) = (\kappa)^T \hat{X}_{q,F_c\tau}(k) \\ \hat{X}_{q,F_c\tau}(k+1) = [\alpha_X \hat{X}_{q,F_c\tau}(k) + \alpha_U U_{F_c\tau}(k) + \alpha_Y \hat{Y}_{q(p)}(k) + \alpha_F \hat{f}_{fuzzy}(p)] \\ + \hat{\delta}_{(p)}(k) + \alpha_P (Y_q(k) - \hat{Y}_{q(p)}(k)) + f(\hat{X}_{q,F_c\tau}(p), U) + I^{-1}(\alpha_P (Y_q(k) - \hat{Y}_{q(p)}(k))) \end{cases} \quad (34)$$

Here, $\tau_{OFLC}(k)$ is the controller output based on the proposed observation-based feedback linearization controller. To improve the reliability of the proposed observation-based feedback linearization fault-tolerant controller, online tuning based on the fuzzy algorithm is proposed. To improve the power of fault reduction in the proposed fault-tolerant control algorithm, the controller coefficients play important roles. Because faults are unknown with respect to various conditions and are difficult to predict, calculating the optimal values for coefficients are complicated. If the controller's coefficients are changed with the condition of the surgical robot for the sinus, the fault could be reduced and eliminated. Thus, for online tuning of the coefficient, a fuzzy algorithm is represented. Based on

Equation (34), the adaptive fuzzy observation-based feedback linearization fault-tolerant controller can be written as the following Equation:

$$\begin{cases} \tau_p(k) = \tau_{onlineFLC}(k) + \hat{Y}_{q(p-online)}(k) \\ \tau_{onlineFLC}(k) = -I(q) \times (\hat{X}_d + \alpha_{p-new}e(k) + \alpha_{d-new}\dot{e}(k) + \alpha_{i-new}\sum e(k)) + f(\hat{X}_{q,F_c\tau(p)}, U) \\ \hat{Y}_{q(p)}(k+1) = (\kappa)^T \hat{X}_{q,F_c\tau(p)}(k) \\ \hat{X}_{q,F_c\tau(p)}(k+1) = [\alpha_X \hat{X}_{q,F_c\tau(p)} + \alpha_U U_{F_c\tau}(k) + \alpha_Y \hat{Y}_{q(p)}(k) + \alpha_F \hat{f}_{fuzzy(p)}] \\ + \hat{\delta}_{(p)}(k) + \alpha_{p-new}(Y_q(k) - \hat{Y}_{q(p)}(k)) + f(\hat{X}_{q,F_c\tau(p)}, U) + I^{-1}(\alpha_{p-new}(Y_q(k) - \hat{Y}_{q(p)}(k))) \end{cases} \quad (35)$$

Here, $\tau_p(k)$, $\tau_{onlineFLC}(k)$, $\hat{Y}_{q(p-online)}(k)$, and $(\alpha_{p-new}, \alpha_{d-new}, \alpha_{i-new})$ are the proposed method for fault-tolerant control in the surgical robot for the sinus, the online tuning part of the feedback linearization controller, the online tuning part of the proposed fuzzy ARX-Laguerre T-S fuzzy robust feedback linearization observer, and the online tuning coefficients, respectively. The online tuning proportional, derivative, and integral coefficients are represented by Equation (36).

$$\begin{cases} \alpha_{p-new} = \alpha_p \times \alpha_{online} \\ \alpha_{d-new} = \alpha_d \times \alpha_{online} \\ \alpha_{i-new} = \alpha_i \times \alpha_{online} \end{cases} \quad (36)$$

where α_{online} is fuzzy output for tuning the proportional, derivative, and integral coefficients. The fuzzy algorithm has two inputs (error and change of error) and one output. The fuzzy membership functions in the interval of $[-0.1, 0.1]$ are Gaussian, and the fuzzy sets are defined as NB, NM, NS, Z, PS, PM, and PB. The fuzzy membership functions for change of error in the interval of $[-2, 2]$ are Gaussian, and the fuzzy sets are defined as NB, NM, NS, Z, PS, PM, and PB. The fuzzy membership functions for fuzzy output in the interval of $[0.1, 2]$ are Gaussian, and the fuzzy sets are defined as PS, PM, and PB. The rule table for online tuning the proposed fuzzy fault-tolerant controller is given in Table 4. Figure 13 illustrates the power of fault-tolerant control in the manipulator of the surgical robot for the sinus for online tuning of the fuzzy observer feedback linearization controller (proposed method), observer-based feedback linearization controller, and classical feedback linearization controller. Regarding the figure, the power of fault reduction in the proposed method is significantly better than with the other two methods. The proposed algorithm for fault diagnosis and the fault-tolerant controller of the surgical robot for the sinus are summarized in Algorithm 1.

Table 4. Fuzzy rule table for online tuning of the proposed fault-tolerant control algorithm.

		Change of Error (de)						
		NB	NM	NS	Z	PS	PM	PB
Error (e)	NB	PB	PB	PB	PB	PM	PS	PS
	NM	PB	PB	PB	PM	PS	PS	PS
	NS	PB	PB	PM	PS	PS	PS	PS
	Z	PB	PM	PS	PS	PS	PS	PS
	PS	PB	PB	PB	PB	PM	PS	PS
	PM	PB	PB	PB	PM	PS	PS	PS
	PB	PB	PB	PM	PS	PS	PS	PS

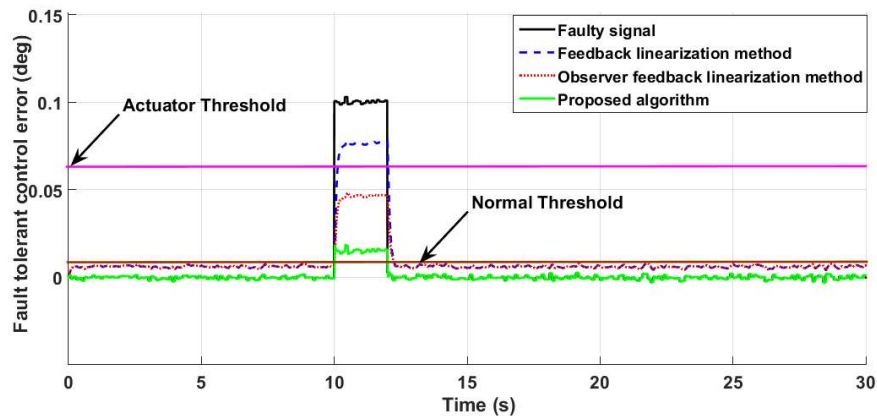


Figure 13. Fault-tolerant control for fuzzy feedback linearization method, observation-based feedback linearization method, and proposed method for a surgical robot for the sinus.

Algorithm 1 Online tuning of the observation-based fuzzy ARX-Laguerre T-S fuzzy robust feedback linearization observer for fault detection, estimation, identification, and tolerant control of a surgical robot for the sinus.

- 1: Run the ARX technique for system modeling (11)
 - 2: Run the extended ARX method using the ARX-Laguerre technique for system modeling (13)
 - 3: Run the extended ARX-Laguerre technique based on fuzzy ARX-Laguerre system modeling (16)
 - 4: Run the fuzzy ARX-Laguerre feedback linearization observer (17), (18)
 - 5: Run the fuzzy ARX-Laguerre robust feedback linearization observer based on the variable structure technique (21), (22)
 - 6: Run the fuzzy ARX-Laguerre T-S fuzzy robust feedback linearization observer (26), (27)
 - 7: Run the residual signal generation (29)
 - 8: Run the threshold generation based on the variable structure technique (30)
 - 9: Run the proposed fault detection algorithm (31)
 - 10: Run the proposed fault estimation technique (27)
 - 11: Run the proposed fault identification method (32)
 - 12: Run the feedback linearization technique (33)
 - 13: Run the extended feedback linearization method based on the observation technique for fault tolerance (34)
 - 14: Run the extended observation-based feedback linearization technique and the adaptive fuzzy observation-based feedback linearization technique for fault tolerance (35), (36)
-

4. Results and Analysis

Figure 2 presents the proposed algorithm for fault diagnosis and fault-tolerant control for the surgical robot for the sinus. The effectiveness of the proposed fuzzy ARX-Laguerre T-S fuzzy robust feedback linearization observer for fault estimation, detection, and identification was compared to the fuzzy ARX-Laguerre robust feedback linearization observer and fuzzy ARX-Laguerre feedback linearization observer.

4.1. Fault Detection, Estimation and Identification

Figure 14 illustrates the residual signal for the surgical robot for the sinus and force torque signals in the normal condition. Based on Figure 14a, this system has a spike at various times, such as 5, 10, 12, 15, and 17 s. These signals are not errors, and the signal rise and fall times are very short.

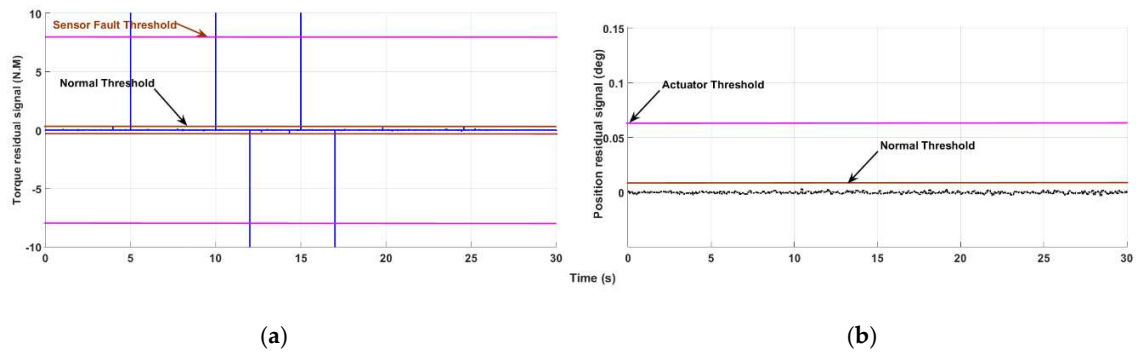


Figure 14. Normal condition residual signals: (a) torque and (b) joint position variable.

Based on Figure 14, in the normal condition, the level of the position residual signal and the torque residual signal should be lower than the normal threshold value. Figures 15–17 illustrate the fault detection in actuator fault, sensor fault, and sensor-actuator fault for the proposed fuzzy ARX-Laguerre T-S fuzzy robust feedback linearization observer, fuzzy ARX-Laguerre robust feedback linearization observer, and fuzzy ARX-Laguerre feedback linearization observer. Based on Figure 16 and Equation (32), in an actuator fault, the position residual signal should be higher than the normal, and the actuator thresholds and torque residual signal should be higher than the normal threshold but lower than the sensor threshold value.

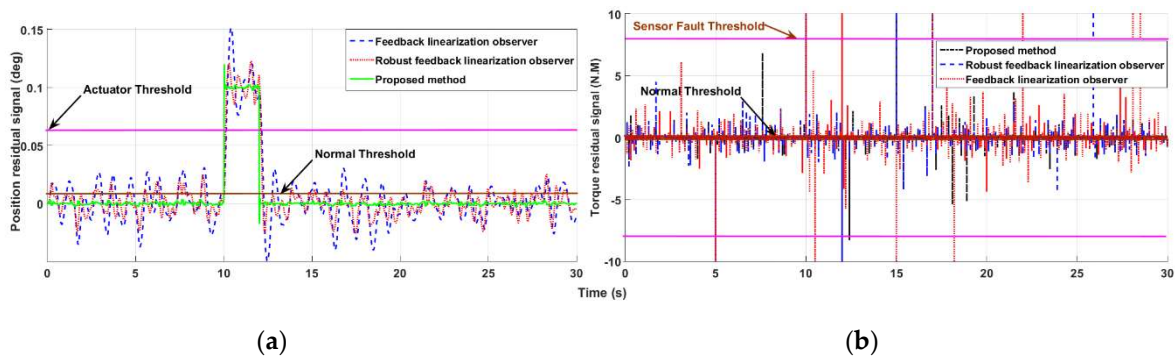


Figure 15. (a) Position residual signals and (b) torque residual signals for actuator fault identification based on the fuzzy ARX-Laguerre feedback linearization method, fuzzy ARX-Laguerre robust feedback linearization method, and fuzzy ARX-Laguerre T-S fuzzy robust feedback linearization method for the surgical robot for the sinus.

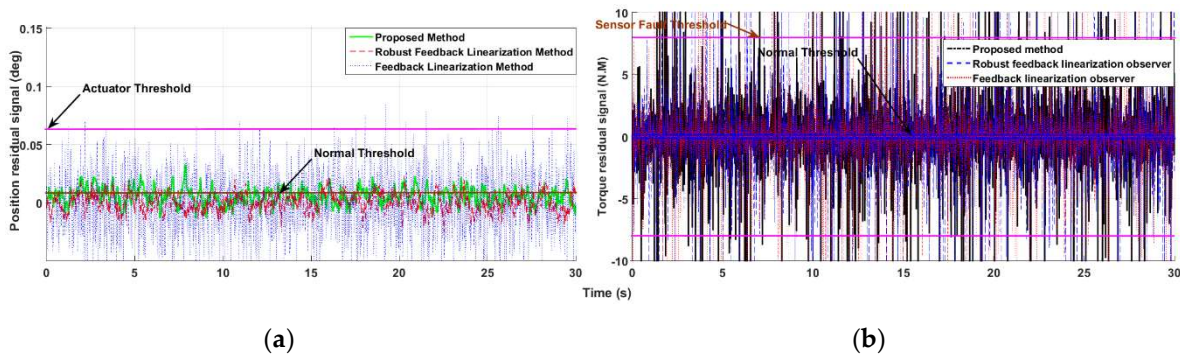


Figure 16. (a) Position residual signals and (b) torque residual signals for sensor fault identification based on the fuzzy ARX-Laguerre feedback linearization method, fuzzy ARX-Laguerre robust feedback linearization method, and fuzzy ARX-Laguerre T-S fuzzy robust feedback linearization method for the surgical robot for the sinus.

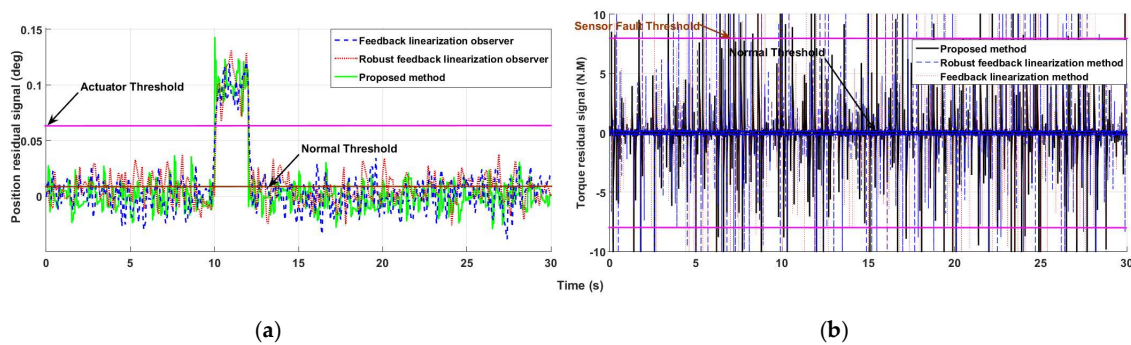


Figure 17. (a) Position residual signals and (b) torque residual signals for **actuator-sensor** fault identification based on the fuzzy ARX-Laguerre feedback linearization method, fuzzy ARX-Laguerre robust feedback linearization method, and fuzzy ARX-Laguerre T-S fuzzy robust feedback linearization method for the surgical robot for the sinus.

Based on Figure 15, the delay time for fault identification in the proposed algorithm is better than with the other techniques. Figure 16 shows the power of sensor fault identification by three methods for the surgical robot for the sinus. Regarding Figure 16a, the classical feedback linearization observer has drawbacks in fault identification in this type of fault. As shown in this figure, the proposed and robust feedback linearization observers have reliable performance compared with the classical feedback linearization observer. Figure 17 illustrates the actuator-sensor fault identification efficiency for the surgical robot for the sinus based on three different algorithms. Regarding this figure, the delay time to fault identification in the proposed method is less than with the other two methods.

4.2. Fault-Tolerant Control

The root mean square (RMS) error of the kinematics and the end-effector position for the surgical robot for the sinus in the normal, actuator fault, sensor failure, and actuator-sensor fault conditions are illustrated in Figures 18–21. Based on Figure 18, the RMS error in the normal condition for the end-effector of the surgical robot for the sinus is close to zero. In Figures 19–21, the error rate is greater than at the normal condition. Regarding these figures, the end-effector positions fluctuate similar to in the normal condition. After fault detection, estimation, and identification based on the fuzzy ARX-Laguerre T-S fuzzy robust feedback linearization (proposed) observer, the proposed fault-tolerant control based on the adaptive fuzzy proposed observation-based feedback linearization controller is tested. To test the proposed fault-tolerant controller, the proposed method is compared with the observation-based feedback linearization controller and the classical feedback linearization control algorithm. The main goal in this part is elimination or reduction of the effect of the fault to increase the rate of successful surgery. Figure 22 shows the effects of the proposed algorithm, the observation-based feedback linearization algorithm, and the classical feedback linearization fault-tolerant controller to reduce/eliminate faults. Based on this figure, the adaptive fuzzy observation-based feedback linearization controller is more reliable for the fault-tolerant controller than the other two methods. The effect of the proposed fault-tolerant algorithm on the RMS error of kinematics end-effector and position is illustrated in Figure 23. Regarding this figure, the proposed technique sharply reduces the RMS error and fluctuation of the end-effector. According to Figures 18 and 23, it is clear that the adaptive fuzzy observation-based feedback linearization control is an active and accurate technique for fault-tolerant control in the surgical robot for the sinus.

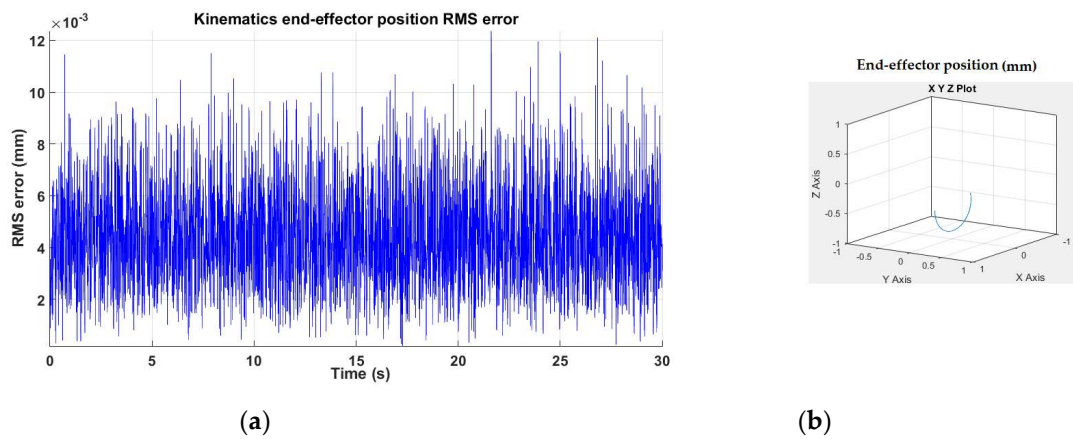


Figure 18. Normal condition: (a) kinematics end-effector position root mean square (RMS) error and (b) end effector position in the XYZ axis.

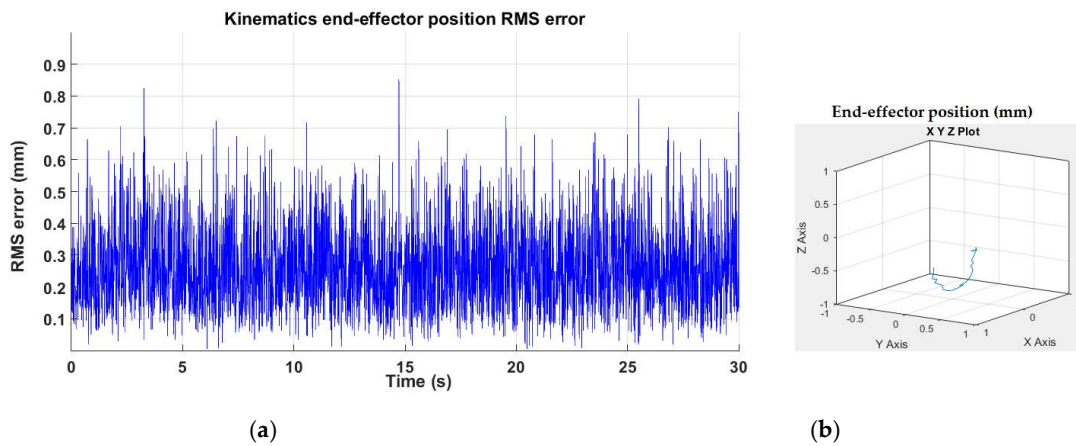


Figure 19. Actuator fault condition: (a) kinematics end-effector position RMS error and (b) end effector position in the XYZ plot.

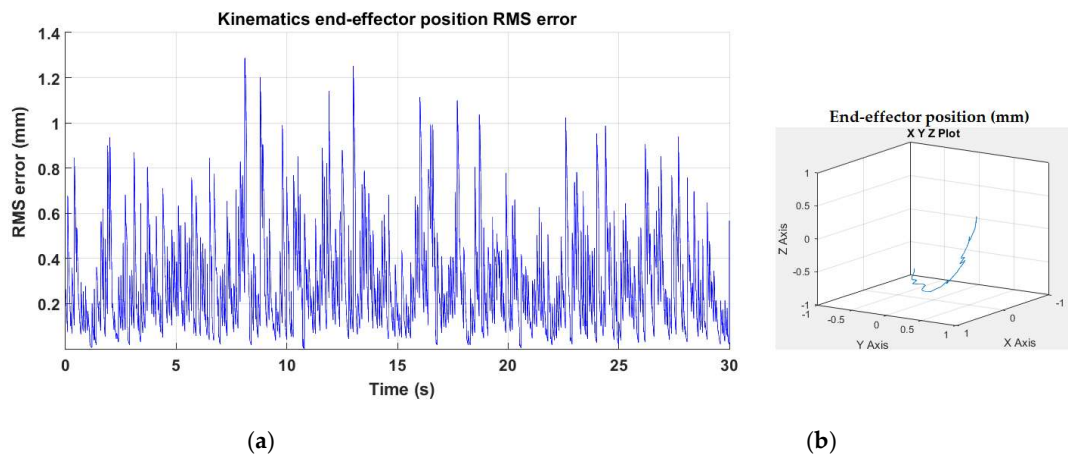


Figure 20. Sensor fault condition: (a) kinematics end-effector position RMS error and (b) end effector position in the XYZ plot.

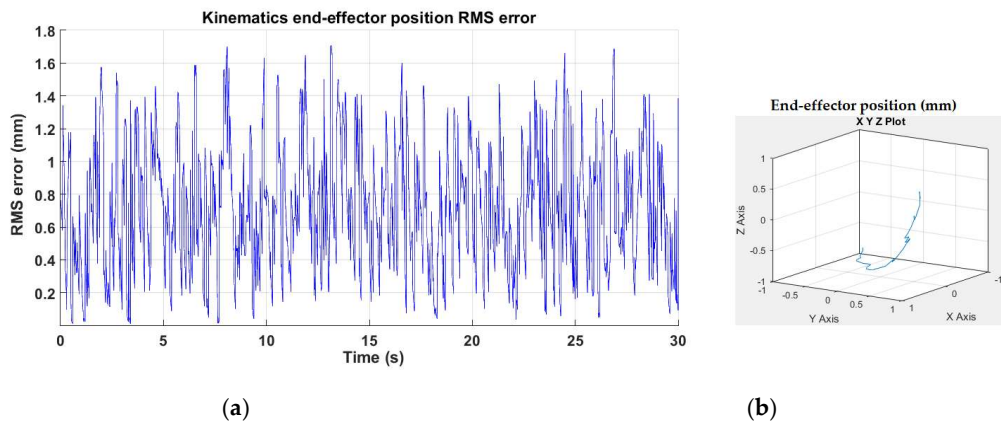


Figure 21. Actuator-sensor fault condition: (a) kinematics end-effector position RMS error and (b) end effector position in the XYZ plot.

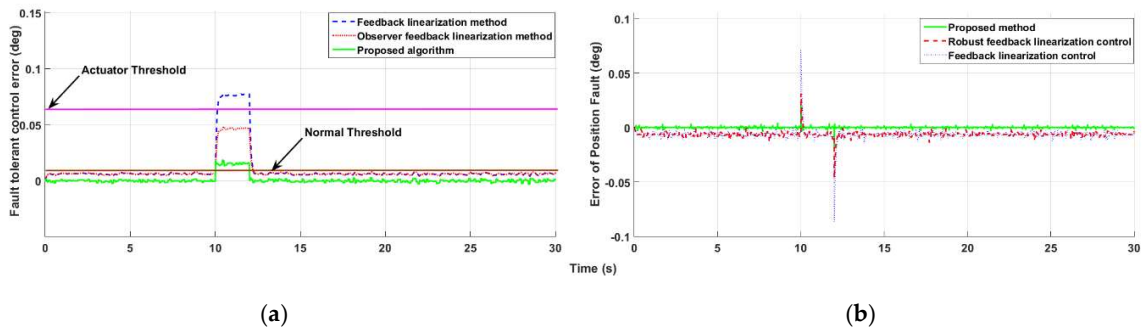


Figure 22. (a) Fault-tolerant control error and (b) error of position fault for the fuzzy feedback linearization method, observation-based feedback linearization method, and proposed method for the surgical robot for the sinus.

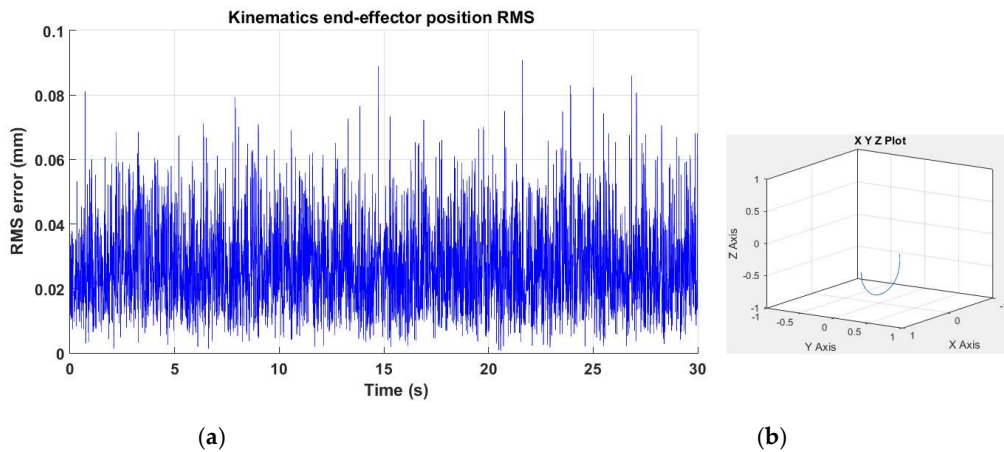


Figure 23. Power of proposed fault-tolerant algorithm for (a) kinematics end-effector position RMS error and (b) end effector position in the XYZ plot.

Figure 24 illustrates the fault-tolerant accuracy of the proposed fault-tolerant controller and feedback linearization fault-tolerant controller in normal and abnormal conditions. This figure illustrates that the minimum error, the average error, and the maximum error for the normal condition with the proposed fault-tolerant controller are 1.8, 2.3, and 3.6 mm, respectively. For the faulty condition using the proposed fault-tolerant algorithm, the errors are 0.8, 2.45, and 7.1 mm, respectively. For the faulty condition using the observer feedback linearization fault-tolerant controller are 6, 8.4, and 20 mm, respectively, and those for the faulty condition with respect to the classical feedback linearization

fault-tolerant controller are 7.3, 35, and 72 mm. According to Figures 22 and 24, the power of fault reduction using the proposed fault-tolerant controller is better than the observer feedback linearization fault-tolerant controller and feedback linearization fault-tolerant controller.

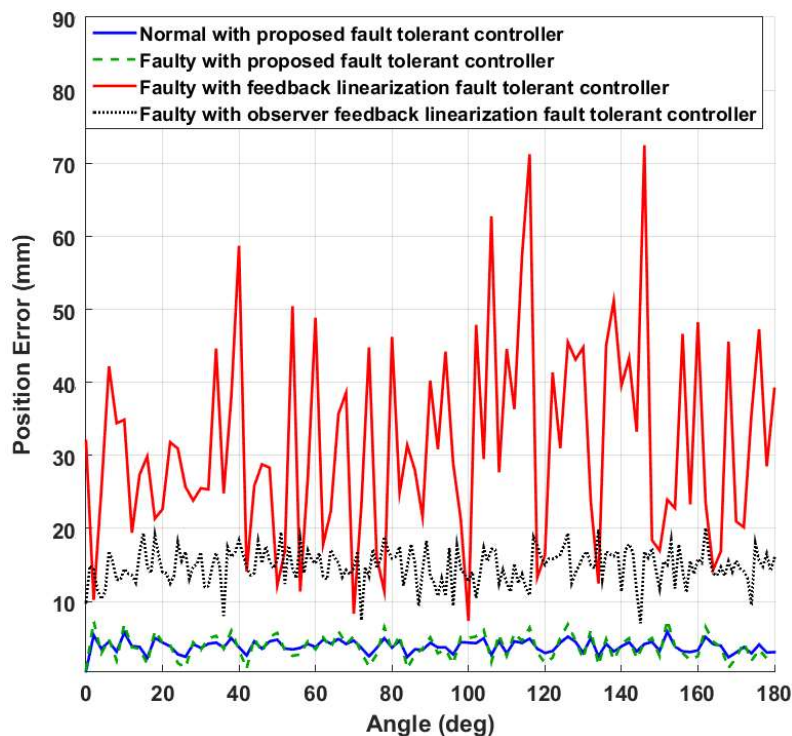


Figure 24. Position error for normal condition, faulty condition with the proposed fault-tolerant controller, faulty condition with the feedback linearization fault-tolerant controller, and faulty condition with the observer feedback linearization fault-tolerant controller.

5. Conclusions

This paper explored a highly accurate, reliable, and robust fault estimation, detection, isolation, and tolerant control for the sinus surgical robot. The proposed method had three main steps: (a) modeling of the surgical manipulator, (b) advanced observer for fault detection, estimation, and isolation, and (c) an advance fault-tolerant controller. In the first step, the surgical manipulator was modeled based on the robust and accurate fuzzy ARX-Laguerre technique. After modeling the maxillary sinus surgical robot, the advanced observer was designed for fault diagnosis. To increase the reliability, robustness, and fault estimation accuracy for fault diagnosis, the fuzzy ARX-Laguerre T-S fuzzy robust feedback linearization observer was designed. After modeling and fault diagnosis for the maxillary sinus surgical robot, the proposed fault-tolerant controller was proposed to reduce the effect of a fault. To increase the robustness and accuracy, an adaptive fuzzy observation-based feedback linearization technique was used in the last step. Regarding the results, the proposed algorithm reduced the average position error from 35 mm to 2.45 mm in the faulty condition. In the future, a hybrid higher-order observation technique will be designed to enhance the performance of fault diagnosis and fault-tolerant control for a surgical robot.

Author Contributions: All the authors contributed equally to the conception of the study, the design of the experiments, the analysis and interpretation of results, and the writing of the manuscript.

Funding: This work was supported by the Korean Institute of Energy Technology Evaluation and Planning (KETEP) and the Ministry of Trade, Industry, and Energy (MOTIE) of the Republic of Korea (No. 20172510102130).

Conflicts of Interest: The authors declare no conflict of interest.

Nomenclature

$i^{-1}T$	Transformation matrix	a_i	distance from \hat{Z}_i to \hat{Z}_{i+1}
α_i	Angle from \hat{Z}_i to \hat{Z}_{i+1}	d_i	distance from \hat{X}_{i-1} to \hat{X}_i
θ_i	Angle from \hat{X}_{i-1} to \hat{X}_i	F_c	force coefficient matrix
τ	Torque	$I(q)$	inertial matrix
$N(q)$	Coefficients of the first-order generalized coordinate matrix	$G(q)$	gravity
δ	Faults and uncertainties	$X_{q,F,\tau}(k)$	state function
$U_{F,\tau}(k)$	State input	$Y_q(k)$	state output
κ	Fourier function	$(W(k-n_W), H(k-n_H))$	system lag
$W(k)$	Output	$H(k)$	input
(λ_W, λ_H)	Coefficients	$e(k)$	zero mean noise
ε	Regressor variables	ψ	coefficient matrix
(α_X, α_U)	Coefficients	$(\alpha_{n,Y} \& \alpha_{n,U})$	Fourier coefficients
(i_Y, i_U)	Robot manipulator order	(λ_Y, λ_U)	function of the Laguerre orthonormal
*	Product of the convolution	$X_{n,Y}(k)$	filter system output
$\chi_{n,U}(k)$	Filter system input	(ζ_a, ζ_b)	orthonormal basis
f_{fuzzy}	Fuzzy function for system estimation	e_m	estimation error
$(H_e^m, H_e^m, H_{fuzzy}^m)$	Fuzzy sets	\dot{e}_m	estimation change of error
$(\alpha_X, \alpha_U, \alpha_Y, \alpha_F)$	Coefficients	$\hat{X}_{q,F,\tau(FLO)}(k)$	state estimation
$\hat{Y}_{q(FLO)}(k)$	Output estimation	$\hat{f}_{fuzzy(FLO)}$	fuzzy estimation function
$\hat{\delta}_{(FLO)}(k)$	Fault estimation	α_p	coefficient
$\hat{X}_{q,F,\tau(FLO)}(k)$	State estimation error	$\hat{\delta}_{(FLO)}(k)$	fault estimation error
$\hat{X}_{q,F,\tau(RFLO)}(k)$	State estimation	$\hat{Y}_{q(RFLO)}(k)$	fuzzy ARX-Laguerre robust feedback linearization output estimation
$\hat{\delta}_{(RFLO)}(k)$	Fault estimation	κ_{VSO}	observer coefficient
$\hat{X}_{q,F,\tau(RFLO)}(k)$	State estimation error	$\hat{\delta}_{(RFLO)}(k)$	fault estimation error
$r_a(k)$	Residual signal for the actuator fault	$r_s(k)$	residual signal for the sensor fault
(TH_a, TH_s)	Threshold values for the actuator and sensor faults	$\hat{\delta}_{fuzzy}(k)$	faulty signal estimator based on the T-S fuzzy algorithm
α_{fuzzy}	Fuzzy coefficient	$(\alpha_{1fuzzy}, \alpha_{2fuzzy}, \alpha_{3fuzzy})$	estimator coefficients for actuator fault, sensor fault, and actuator-sensor fault
$\hat{X}_{q,F,\tau(p)}(k)$	Proposed observer for state estimation	$\hat{Y}_{g(p)}(k)$	proposed observers for output estimation
$\hat{\delta}_{(p)}(k)$	Proposed fault estimation	$\hat{X}_{q,F,\tau(p)}(k)$	proposed state estimation error
$\hat{\delta}_{(p)}(k)$	Proposed fault estimation error	TH_N	threshold value for normal condition
$(\alpha_N, \alpha_a, \alpha_s, \lambda_N, \lambda_a, \lambda_s)$	Coefficients of the sliding mode algorithm in different states	r_N	residual signal for normal condition
\dot{r}_N	Change of residual signal for normal condition	$\sum r_N$	integral of residual signal for normal condition
r_a	Residual signal for actuator fault	\dot{r}_a	change of residual signal for actuator fault
$\sum r_a$	Integral of residual signal for actuator fault	r_s	residual signal for sensor fault
\dot{r}_s	Change of residual signal for sensor fault	$\sum r_s$	integral of residual signal for sensor fault
τ_{FLC}	Controller's torque based on the conventional feedback linearization control	$(\alpha_p, \alpha_d, \alpha_i)$	controller coefficients
$\tau_{OFLC}(k)$	Controller output based on the proposed observation-based feedback linearization controller	$\tau_p(k)$	proposed method for fault-tolerant control
$\tau_{onlineFLC}(k)$	Online tuning part of the feedback linearization controller	$\hat{Y}_{g(p-online)}(k)$	online tuning part of the proposed method
$(\alpha_{p-new}, \alpha_{d-new}, \alpha_{i-new})$	Online tuning coefficients	α_{online}	fuzzy output for tuning the proportional, derivative, and integral coefficients

References

1. Bell, G.W.; Joshi, B.B.; Macleod, R.I. Maxillary sinus disease: Diagnosis and treatment. *Br. Dent. J.* **2011**, *210*, 113. [CrossRef] [PubMed]
2. Minovi, A.; Kollert, M.; Draf, W.; Bockmühl, U. Inverted papilloma: Feasibility of endonasal surgery and long-term results of 87 cases. *Rhinology* **2006**, *44*, 205–210. [PubMed]
3. Hong, W.; Xie, L.; Liu, J.; Sun, Y.; Li, K.; Wang, H. Development of a novel continuum robotic system for maxillary sinus surgery. *IEEE/ASME Trans. Mechatron.* **2018**, *23*, 1226–1237. [CrossRef]
4. Xie, L.; Kemp, C.D.; Yang, S.C. The simulator development of cardiovascular interventional virtual surgery with force feedback. *J. Jiangxi Norm. Univ.* **2017**, *4*, 331–337.
5. Wu, L.; Song, S.; Wu, K.; Lim, C.M.; Ren, H. Development of a compact continuum tubular robotic system for nasopharyngeal biopsy. *Med. Biol. Eng. Comput.* **2017**, *55*, 403–417. [CrossRef] [PubMed]
6. Zheng, L. Design of a novel flexible endoscope–cardioscope. *J. Mech. Robot.* **2016**, *8*, 051014.
7. Wang, H.; Wang, C.; Chen, W.; Liang, X.; Liu, Y. Three-dimensional dynamics for cable-driven soft manipulator. *IEEE/ASME Trans. Mechatron.* **2017**, *22*, 18–28. [CrossRef]

8. Ma, H.-J.; Yang, G.-H. Simultaneous fault diagnosis for robot manipulators with actuator and sensor faults. *Inf. Sci.* **2016**, *366*, 12–30. [[CrossRef](#)]
9. Van, M.; Ge, S.S.; Ren, H. Finite time fault-tolerant control for robot manipulators using time delay estimation and continuous nonsingular fast terminal sliding mode control. *IEEE Trans. Cybern.* **2017**, *47*, 1681–1693. [[CrossRef](#)]
10. Xiao, B.; Shen, Y. An intelligent actuator fault reconstruction scheme for robotic manipulators. *IEEE Trans. Cybern.* **2018**, *48*, 639–647. [[CrossRef](#)]
11. Van, M.; Pasquale, F.; Dariusz, C. Fault diagnosis and fault-tolerant control of uncertain robot manipulators using high-order sliding mode. *Math. Probl. Eng.* **2016**, *2016*, 7926280. [[CrossRef](#)]
12. Kamel, M.A.; Yu, X.; Zhang, Y. Fault-tolerant cooperative control design of multiple wheeled mobile robots. *IEEE Trans. Control Syst. Technol.* **2018**, *26*, 756–764. [[CrossRef](#)]
13. Li, S.; Song, Y.; Zhou, G. Leak detection of water distribution pipeline subject to failure of socket joint based on acoustic emission and pattern recognition. *Measurement* **2018**, *115*, 39–44. [[CrossRef](#)]
14. Gao, Y.; Liu, Y.; Ma, Y.; Cheng, X.; Yang, J. Application of the differentiation process into the correlation-based leak detection in urban pipeline networks. *Mech. Syst. Signal Process.* **2018**, *112*, 251–264. [[CrossRef](#)]
15. Xu, L.; Cao, M.; Song, B.; Zhang, J.; Liu, Y.; Alsaadi, F.E. Open-circuit fault diagnosis of power rectifier using sparse autoencoder based deep neural network. *Neurocomputing* **2018**, *311*, 1–10. [[CrossRef](#)]
16. Cecati, C. A survey of fault diagnosis and fault-tolerant techniques—Part II: Fault diagnosis with knowledge-based and hybrid/active approaches. *IEEE Trans. Ind. Electron.* **2015**, *62*, 3752–3756.
17. Hoang, D.-T.; Kang, H.-J. A survey on Deep Learning based bearing fault diagnosis. *Neurocomputing* **2019**, *335*, 327–335. [[CrossRef](#)]
18. Piltan, F.; Kim, C.-H.; Kim, J.-M. Advanced Adaptive Fault Diagnosis and Tolerant Control for Robot Manipulators. *Energies* **2019**, *12*, 1281. [[CrossRef](#)]
19. Ravandi, A.K.; Khanmirza, E.; Daneshjou, K. Hybrid force/position control of robotic arms manipulating in uncertain environment based on adaptive fuzzy sliding mode control. *Appl. Soft Comput.* **2018**, *70*, 864–874. [[CrossRef](#)]
20. Zhang, T.; Tan, Y.; Zhang, X.; Zhao, J. A novel hybrid technique for leak detection and location in straight pipelines. *J. Loss Prev. Process Ind.* **2015**, *35*, 157–168. [[CrossRef](#)]
21. Najeh, T.; Njima, C.B.; Garna, T.; Ragot, J. Input fault detection and estimation using PI observer based on the ARX-Laguerre model. *Int. J. Adv. Manuf. Technol.* **2017**, *90*, 1317–1336. [[CrossRef](#)]
22. Bouzrara, K.; Garna, T.; Ragot, J.; Messaoud, H. Decomposition of an ARX model on Laguerre orthonormal bases. *ISA Trans.* **2012**, *51*, 848–860. [[CrossRef](#)] [[PubMed](#)]
23. Piltan, F.; Kim, J.-M. Bearing fault diagnosis by a robust higher-order super-twisting sliding mode observer. *Sensors* **2018**, *18*, 1128. [[CrossRef](#)] [[PubMed](#)]
24. Li, X.; Mba, D.; Diallo, D.; Delpha, C. Canonical Variate Residuals-Based Fault Diagnosis for Slowly Evolving Faults. *Energies* **2019**, *12*, 726. [[CrossRef](#)]
25. Fuentes-García, M.; Maciá-Fernández, G.; Camacho, J. Evaluation of diagnosis methods in PCA-based Multivariate Statistical Process Control. *Chemom. Intell. Lab. Syst.* **2018**, *172*, 194–210. [[CrossRef](#)]
26. Piltan, F.; Kim, J.-M. Bearing Fault Diagnosis Using an Extended Variable Structure Feedback Linearization Observer. *Sensors* **2018**, *18*, 4359. [[CrossRef](#)] [[PubMed](#)]
27. Piltan, F.; Kim, J.-M. Nonlinear Extended-state ARX-Laguerre PI Observer Fault Diagnosis of Bearings. *Appl. Sci.* **2019**, *9*, 888. [[CrossRef](#)]
28. Li, L.; Ding, S.X.; Qiu, J.; Yang, Y. Real-time fault detection approach for nonlinear systems and its asynchronous T–S fuzzy observer-based implementation. *IEEE Trans. Cybern.* **2017**, *47*, 283–294. [[CrossRef](#)]
29. Li, L.; Chadli, M.; Ding, S.X.; Qiu, J.; Yang, Y. Diagnostic observer design for t–s fuzzy systems: Application to real-time-weighted fault-detection approach. *IEEE Trans. Fuzzy Syst.* **2018**, *26*, 805–816. [[CrossRef](#)]
30. Li, L.; Ding, S.X.; Qiu, J.; Yang, Y.; Xu, D. Fuzzy observer-based fault detection design approach for nonlinear processes. *IEEE Trans. Syst. Man Cybern. Syst.* **2017**, *47*, 1941–1952. [[CrossRef](#)]
31. Abbaspour, A.; Aboutalebi, P.; Yen, K.K.; Sargolzaei, A. Neural adaptive observer-based sensor and actuator fault detection in nonlinear systems: Application in UAV. *ISA Trans.* **2017**, *67*, 317–329. [[CrossRef](#)]
32. Tayebi-Haghighi, S.; Piltan, F.; Kim, J.-M. Robust Composite High-Order Super-Twisting Sliding Mode Control of Robot Manipulators. *Robotics* **2018**, *7*, 13. [[CrossRef](#)]

33. Hosseinzadeh, M.; Salmasi, F.R. Fault-tolerant supervisory controller for a hybrid AC/DC micro-grid. *IEEE Trans. Smart Grid* **2018**, *9*, 2809–2823. [[CrossRef](#)]
34. Tan, N.; Gu, X.; Ren, H. Pose Characterization and Analysis of Soft Continuum Robots with Modeling Uncertainties Based on Interval Arithmetic. *IEEE Trans. Autom. Sci. Eng.* **2018**, *99*, 1–15. [[CrossRef](#)]
35. Tatlicioglu, E.; Walker, I.D.; Dawson, D.M. Dynamic modelling for planar extensible continuum robot manipulators. In Proceedings of the 2007 IEEE International Conference on Robotics and Automation, Roma, Italy, 10–14 April 2007; pp. 1357–1362.
36. Piltan, F.; Eram, M.; Taghavi, M.; Sadrnia, O.R.; Jafari, M. Nonlinear Fuzzy Model-base Technique to Compensate Highly Nonlinear Continuum Robot Manipulator. *Int. J. Intell. Syst. Appl.* **2013**, *5*, 135–148. [[CrossRef](#)]
37. Piltan, F.; TayebiHaghighi, S.; Jowkar, S.; Bod, H.R.; Sahamijoo, A.; Heo, J.-S. A Novel Intelligent ARX-Laguerre Distillation Column Estimation Technique. *Int. J. Intell. Syst. Appl.* **2019**, *11*, 52–60. [[CrossRef](#)]



© 2019 by the authors. Licensee MDPI, Basel, Switzerland. This article is an open access article distributed under the terms and conditions of the Creative Commons Attribution (CC BY) license (<http://creativecommons.org/licenses/by/4.0/>).